ORIGINAL ARTICLE

Feature-driven LSTM model for earthquake-based anomaly detection in noisy environments

Gürhan Tokgöz · Eda Avanoğlu Sıcacık

Received: 20 December 2024 / Accepted: 8 November 2025
© The Author(s) 2026

Abstract

This study uses a ground motion recorder to measure surface vibrations and analyzes patterns to enhance earthquake prediction. Surface vibrations caused by far-focus earthquakes were recorded, and their responses in the temporal and frequency domains were evaluated. A recurrent unsupervised artificial neural network model, validated through feature extraction studies, was developed to predict pattern changes during earthquakes. A secondary objective was to assess the impact of strong sinusoidal vibrations from turbine and hydro generator-induced rotational motion on the resonance state of bedrock beneath the Gürsöğüt Hydroelectric Dam. Continuous ground motion data collected from July 2023 to October 2024 included 20 far-focus earthquakes with magnitudes between 4.2 and 5.6. A Long Short-Term Memory (LSTM) deep learning model was trained incrementally using spectral and statistical features from 19 earthquakes to predict the excluded one in a repeated evaluation. Using 5-s sliding windows, the model forecasted anomalies approximately 50 s before each earthquake. The deep learning approach successfully predicted seismic events by recognizing patterns in spectral and statistical features before and during earthquakes. This revealed directional and magnitude relationships that generalize seismic behavior. The model correctly identified approximately 64% of actual seismic peaks (true positives) while misclassifying about 18% of non-seismic peaks as seismic (false positives). The Mean Absolute Error (MAE) in non-peak zones was 0.254, indicating effective background noise suppression. These results suggest the model effectively suppresses background noise while focusing on meaningful seismic activity. These results demonstrate that the model effectively suppresses background noise while focusing on meaningful seismic activity. Emphasizing feature identification over predictive tasks, the study provides a framework for labeling seismic event anomalies before and during earthquakes and designing attention mechanisms in machine and deep learning models. The model offers a generalized understanding of seismic behavior by incorporating seismic traces from different fault lines. Additionally, its ability to determine the natural frequency of bedrock supports improved soil–foundation interaction modeling, which is critical for large-scale structures.

Keywords Surface vibration · Seismic signal processing · Spectral feature extraction · LSTM neural networks

1 Introduction

Earthquakes are sudden and destructive natural phenomena caused by deep tectonic movements within the Earth's crust. The high-magnitude earthquakes on 6 February 2023 in southeastern Türkiye demonstrated the devastating effects of complex fault interactions in seismically active regions. According to the Disaster and Emergency Management Authority (AFAD), these earthquakes affected 11 provinces and resulted in more than 50,500 fatalities [1].

Earthquake predictors have become a critical focus of scientific research due to their unpredictability and wide-ranging impacts. Although these efforts have taken various forms throughout history, they became systematic modern scientific methods, particularly in the mid-twentieth century. During the 1960s, which was considered the starting point of contemporary earthquake prediction studies, countries such as Japan and the United States conducted extensive research in this field. Scientists developed various theories and models to predict seismic activity [2–4].

These early studies aimed to understand the triggering mechanisms of earthquakes and identify the indicators these mechanisms produced. For instance, investigating precursory tremors, gas emissions, crustal deformations, and magnetic field variations formed the foundation of earthquake prediction. However, the accuracy and reliability of these indicators still need to be further studied. The difficulties of earthquake prediction arise from the complex characteristics of these natural phenomena; the factors triggering earthquakes typically involve numerous interrelated variables. Therefore, earthquake prediction remains a crucial scientific challenge.

Current approaches used for the prediction of earthquakes are divided into long-term and short-term predictions. Long-term predictions [5, 6] estimate the general probability of seismic activity in a specific region, while short-term predictions aim to determine the location, timing, and magnitude of an impending earthquake. Recent technological advancements have provided a substantial and novel dimension to these attempts. Technologies including artificial intelligence, machine learning, and big data analysis yield promising results in earthquake prediction. For instance, algorithms designed to address the non-linear nature of seismic data and extract meaningful features enable more precise analysis of seismic events.

Current studies on earthquake prediction can be primarily classified based on the methodologies employed, including mathematical analysis, precursor signal research, machine learning algorithms, and deep learning techniques.

Seismic wave movements vary depending on factors such as the earthquake's magnitude, focal depth, soil condition, and the characteristics of the fault line where the earthquake occurs. Precursor waves occur at different intensities and frequencies in each earthquake, and soil properties influence wave transmission. Thus, the same earthquake produces distinct signal characteristics in different regions. P-waves may overlap with more pronounced S-waves or surface waves. When considering these factors, the validity of the assumptions used in traditional prediction methods for all earthquake scenarios is challenging.

However, artificial intelligence, such as machine learning and deep learning, has shown promising results, particularly in time series prediction within data engineering. These methods enhance the ability to detect traces, trends, and abnormal and chaotic conditions in seismic data often overlooked by traditional techniques.

Convolutional Neural Networks (CNN) and Long Short-Term Memory (LSTM) models stand out for their ability to analyze spatial and temporal relationships in complex seismic data among deep learning methods. Koehler et al. [7] employed CNN-based high-sampling-rate GNSS data to predict earthquakes in Japan. Their findings demonstrated that high-speed GNSS-based positional data effectively captures spatial features. Similarly, [8] combined LSTM and CNN models to process spatial information and time series of seismic regions. This hybrid modeling approach highlighted the effectiveness of CNNs in spatial feature extraction and LSTMs in temporal analysis, ultimately improving prediction accuracy in complex datasets.

Jena et al. [9] trained a CNN-based model using features such as magnitude, epicenter, depth, and frequency from past earthquakes. The results of this model were successful in the prediction of the frequency and magnitude

of aftershocks. Moreover, Mousavi and Beroza [10] employed a CNN model to estimate earthquake locations using single-station seismogram records. Their method focused on predicting epicenter distances and precursor waves. They noted that this approach could be effectively used for rapid earthquake source characterization based on limited observations and for locating sparsely recorded earthquakes.

LSTM models have achieved significant success in earthquake prediction due to their ability to process sequential and temporal data effectively. Berhich et al. [11] developed an attention-based LSTM model that accurately predicted earthquake timing, magnitude, and location in regions with moderate seismic activity. The ability of the model to focus on significant patterns in time series data improved accuracy. Bhandarkar et al. [12] compared LSTM, a type of Recurrent Neural Network (RNN), with a Feedforward Neural Network (FFNN) using historical earthquake location and magnitude data. It was shown that LSTM was more effective due to its consideration of temporal dependencies in sequential data.

Another critical study [13] presented a Bidirectional LSTM model that integrated the multidimensional characteristics of earthquakes. The model was trained by considering variations between successive earthquake records, providing a robust framework for prediction. Besides, [14, 19] analyzed the performance of time-series models using acceleration time data. The findings of the analyses highlighted LSTM's superior performance in datasets prone to temporal information loss.

Henriquez et al. [15] demonstrated that LSTM models could accurately predict earthquake magnitudes using data from a single station. This method has shown efficacy despite limited data availability. Furthermore, Abdalzaher et al. [16] emphasized LSTM's ability to rapidly provide reliable earthquake parameter predictions using single-station data, especially in scenarios with constrained datasets. Rusho et al. [17] integrated LSTM with attention mechanisms and other algorithms to deliver high-performance predictions on large-scale datasets. This model was exceptionally proficient in predicting ground acceleration, which was considered a crucial contributor to on-site early warning systems.

Wang et al. [18] emphasized LSTM's capacity to assess temporal dependencies, enabling improved accuracy in predicting sequential events during or following earthquakes. Wang et al. [14, 19] showed that LSTM could precisely estimate the arrival times of P and S waves, providing rapid and reliable results. In a similar study, [20] demonstrated the effectiveness of LSTM-based predictive systems in disaster management in high-risk areas by providing long-term data analysis and enhancing prediction accuracy. Integrating LSTM models with sensor networks [21] enables real-time data collection and analysis, improving the efficiency of early warning systems. The recent study [22] focused on LSTM for time series analysis in clustering-based prediction algorithms. The study classified seismic data according to spatial and temporal characteristics, exploring the recurrence probabilities of sequential earthquakes and identifying temporal patterns.

These studies collectively underscore the versatility and effectiveness of LSTM models in capturing and leveraging temporal dependencies in seismic data, offering innovative solutions for earthquake prediction, early warning systems, and disaster management.

Despite recent advancements, many existing approaches still face significant limitations in real-world earthquake prediction. Traditional methods often rely on macro-level seismic parameters such as epicenter, depth, and magnitude. As a result, their effectiveness in short-term forecasting remains limited. Although useful, early warning systems depend solely on detecting P waves. This restricts alerts to just a few seconds after the earthquake has already started. Additionally, detecting P waves in noisy environments is technically challenging, which reduces spatial coverage and decreases timing precision.

Physically based models also struggle with high data demands, regional geological calibration requirements, and limited generalizability. Similarly, low signal-to-noise ratios, sensor limitations, and signal instability challenge raw time series approaches, which reduce model robustness across varying geophysical conditions. While classical RNNs can, in theory, model sequential dependencies, they tend to fail with long-term dependencies due to vanishing gradient issues. In contrast, LSTMs, with their gated memory mechanisms, are better equipped to capture evolving structural signal patterns, particularly pre-seismic spectral and statistical anomalies.

This study proposes a hybrid framework integrating the Local Outlier Factor (LOF) algorithm with an LSTM model to address these challenges. No previous study has applied a LOF + LSTM combination to non-time-series spectral and statistical features for anomaly detection in high-noise environments, particularly those influenced by turbine-induced vibrations. This represents a significant research gap in current earthquake prediction literature. The model enables robust anomaly detection even in noisy environments by extracting abstract yet representative features, such as entropy, frequency distribution, statistical moments, and inter-channel correlations. LOF's sensitivity to local density variations and distribution-free nature further supports generalizability across diverse seismic conditions. Unlike conventional methods, the proposed approach performs regression-based prediction of LOF-derived anomaly scores using non-time-series spectral and statistical features obtained from ground motion data affected by turbine-induced noise. This methodological innovation is particularly relevant for engineering applications, where effective preprocessing is essential to reveal meaningful patterns in high-noise environments.

2 The determination of the study area

A region near the Gürsöğüt dam and hydroelectric power plant was chosen for measurements under specific conditions: the presence of a known external source of activity (electricity generation), an area without noisy conditions from an unknown source, and it is directly located on granodiorite bedrock.

Major dams are typically constructed on bedrock to ensure structural integrity and minimize differential settlement. The mechanical stability of such structures is closely tied to the orientation and composition of the underlying geological layers [23]. Sedimentary soils, which are often heterogeneous and deformable, tend to attenuate seismic energy due to internal friction and irregular layering. In contrast, due to its homogeneous and rigid nature, bedrock transmits seismic waves over longer distances with minimal energy loss [24]. This characteristic improves the accuracy and consistency of ground motion recordings, making bedrock-based monitoring sites highly suitable for seismic analysis.

In hydroelectric power plants, mechanical components such as turbines, generators, and pumps produce periodic ground vibrations. These vibrations occur at near-constant frequencies due to the continuous energy input during electricity production. Because this excitation is predictable and sustained, it is ideal for examining how the ground responds to steady-state vibrational loading. Such controlled environments are beneficial for studying resonance behavior and identifying dominant subsurface frequencies, particularly in cases where the response of the underlying bedrock is the primary focus.

The experimental study showed that ground response was significantly amplified due to resonance when sinusoidal waves were applied at the natural frequency of the ground [25]. Building on this finding, the current study focuses on identifying the resonance conditions of the bedrock by matching external excitation frequencies with the ground's natural frequency. The aim is to determine the dominant frequency of the soil profile in areas surrounding hydroelectric power plants with sustained energy production.

A Force Balance type three-axis strong ground motion recorder was used to collect continuous data at a sampling rate of 100 Hz. The device was installed on bedrock and operated between July 1, 2023, and October 30, 2024.

During this period, 20 shallow earthquakes with magnitudes ranging from 4.2 to 5.6 were recorded, originating from distant sources. The locations of these events are presented in Fig. 1, while their magnitudes and focal depths are listed in Table 1. The continuous data were analyzed in two-hour intervals, including the time windows surrounding each earthquake.



Fig. 1 Measurement point and location of recorded earthquakes (Red: Gauge, Blue: Earthquakes)

Table 1 Characteristics of earthquakes recorded

Date/ Time (UTC)	Epicenter (City)	Magnitude (Mw)	Focal depth (km)
2024-11-07/ 03:24	Afyon	4.2	7
2023-12-2/16:04	Çankırı	4.7	9
2024-01-25/13:04	Malatya	5.2	8
2023-11-23/14:49	Malatya	4.6	8
2024-10-16/ 07:46	Malatya	5.9	10.4
2024-01-27/ 05:19	Izmir	5	10
2024-03-10/13:55	Akdeniz	4.8	21
2024-03-21/19:20	Balıkesir	4	7.7
2024-05-23/14:57	Çorum	4.4	13
2024-06-24/ 22:36	Manisa	4.7	10
2024-07-22/14:39	Çanakkale	4.5	10
2024-03-04/18:38	Çanakkale	4.8	10
2024-08-03/ 02:05	Bursa	4	4.7
2023-12-04/ 07:42	Bursa	5.1	5.4
2023-07-25/ 05:44	Kozan	5.5	12
2024-10-27/17:07	Kozan	5	9.7
2023-08-01/15:06	Selçuklu	4.8	10
2023-08-29/ 04:58	Kulu	4.8	10.7
2023-10-14/14:07	Bolu	4.6	5
2024-04-18/15:11	Tokat	5.6	7.3

3 Methodology

3.1 Data analyses

The time-domain datasets representing earthquake events include different scenarios, such as earthquakes in noise-free environments, earthquakes in turbine operation, and when a turbine suddenly stops or starts during an earthquake. Time-domain data show only the relationship between amplitude and time. As a result, detecting low-amplitude and continuous signal components is challenging using acceleration-time graphs alone.

In time-series analysis, frequency-based methods, particularly the Fourier Transform and Power Spectral Density (PSD) analysis, are critical for enhancing spectral resolution due to their ability to observe the energy density of a signal in the frequency domain [26].

Spectrograms further decompose the signal into frequency components, indicating which frequencies are active, when, and for how long. These methods detect short-term embedded patterns and continuous effects in the frequency domain that might be imperceptible in the time series.

Figure 2 presents the acceleration-time graph recorded during the 5.2 magnitude earthquake in Malatya. The event occurred around the 6500th second, during a noisy period when the turbine was operational. As a result, the earthquake-induced vibrations were indistinguishable from the background noise in the time-domain graph. However, the corresponding spectrogram clearly shows two separate frequency components: a fixed range (17–30 Hz) related to turbine operation, and transient low-frequency components (0–3 Hz) associated with the earthquake.

In Fig. 3, the acceleration-time graph revealed that the turbine started operating around 1666 s and stopped at nearly 6153 s. During the operational period, the spectrogram displayed dense, continuous line-like features. These were associated with stable sinusoidal signals generated by rotating machine components operating at a constant speed. Such signals appeared as thin, regular lines at specific frequencies, reflecting the prolonged and uniform vibration pattern caused by turbine activity.

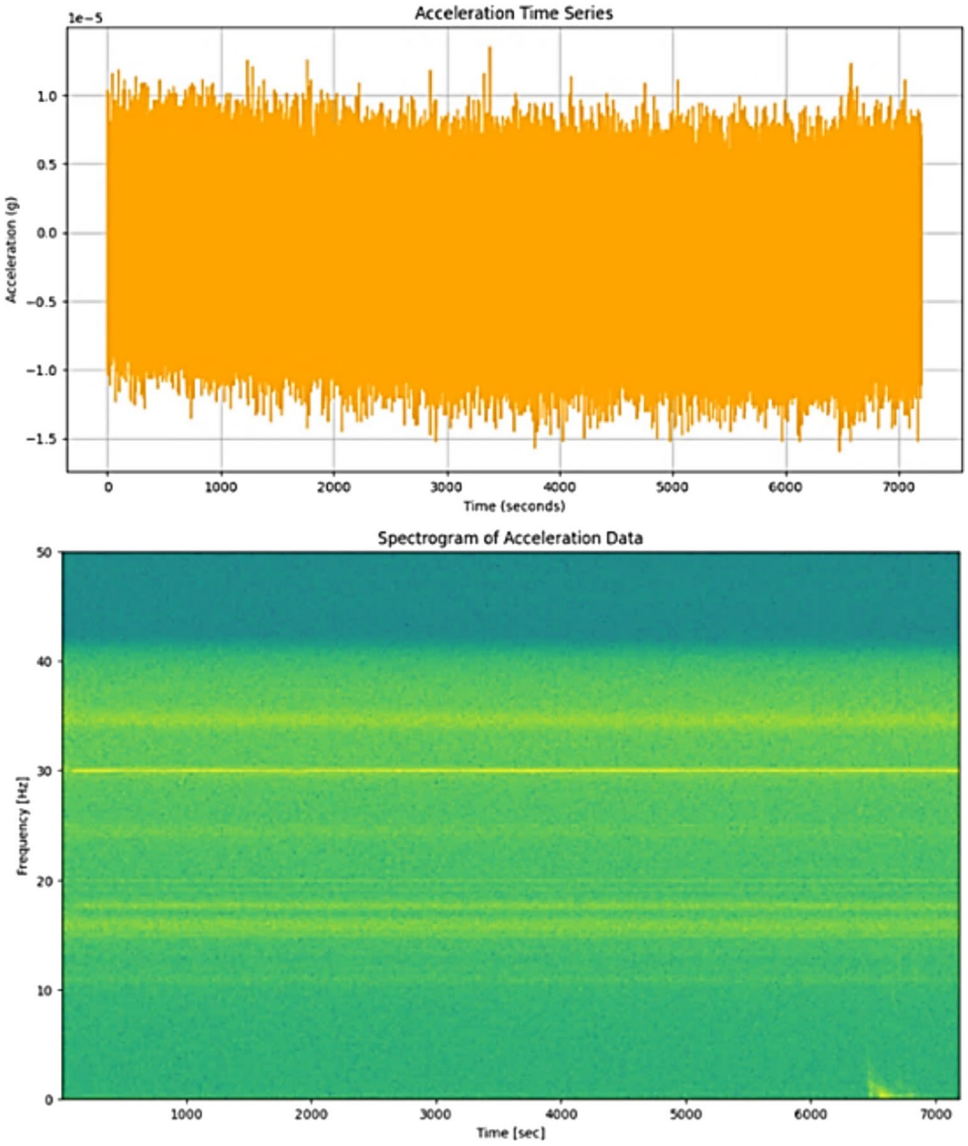


Fig. 2 Malatya earthquake (23.11.2023) acceleration time graph

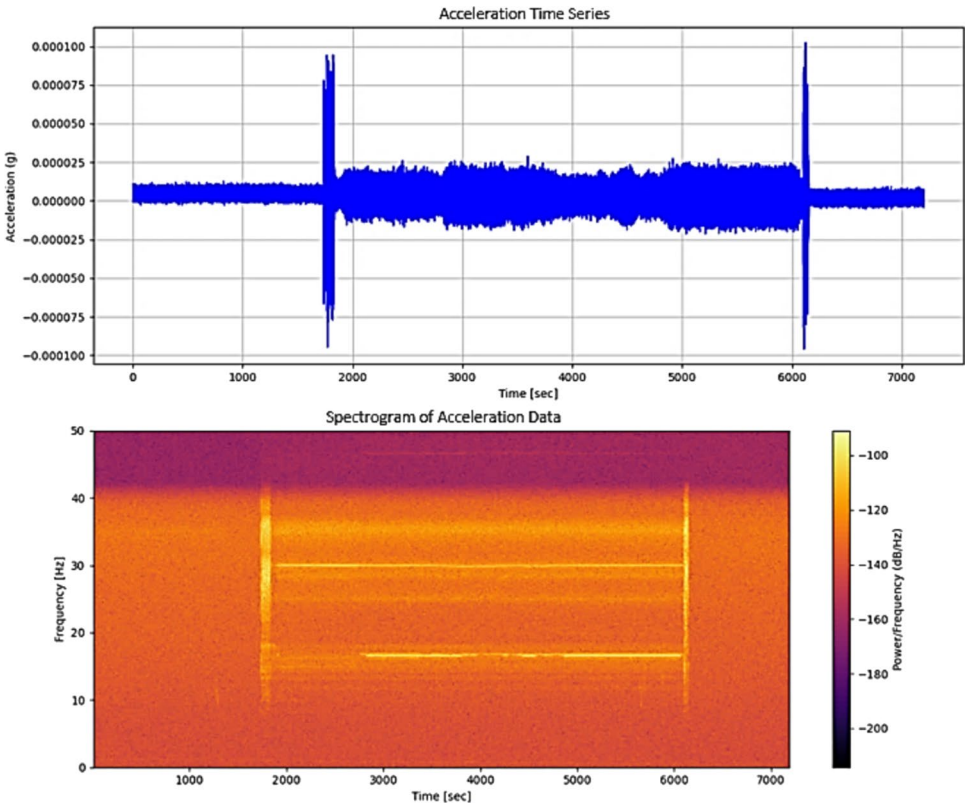


Fig. 3 Turbine operating status impacts

Strong and consistent frequency components around 17 Hz and 30 Hz were observed, which are associated with turbine operation. In addition, broader and less intense spectral components appeared near 25 Hz and 35 Hz. These were independent frequencies, characterized by lower intensity and wider dispersion.

Figure 4 presents the acceleration-time graph showing that the turbine was shut down between 115 and 625 s. Spectrogram analysis revealed that the 25 Hz frequency component continued for a short duration even after the turbine had stopped. This observation may be explained by the physical properties of hard rock formations, which can retain vibrational energy and continue oscillating at their natural frequencies for a limited time after the external excitation ends.

Rock resonances tend to become more pronounced when triggered by external forces and can persist at different frequencies depending on the structural properties of the rock [24]. Frequencies with broad spectral bandwidths observed in the spectrograms may correspond to the system's natural frequencies. Given that the measurements were taken on granodiorite, a dense and rigid rock formation, this broad frequency distribution is likely related to the natural resonance characteristics of the site.

PSD graphs were utilized to analyze frequency variations in the bedrock and investigate the characteristic properties. These graphs presented valuable data for comparison with the frequency intensities of turbine operational conditions, earthquakes, and sudden turbine start/stop events. PSD graphs facilitate the analysis of energy distribution across specific frequency ranges, making them essential tools for identifying patterns in frequency patterns [26].

Figure 5 shows the acceleration-time graph of a recording that includes an earthquake and a turbine shutdown event. The following time intervals correspond to specific phenomena:

- 4076–4153 s: Earthquake event,
- 4461–4923 s: Sudden turbine shutdown,
- 4980–4990 s: Amplitudes immediately following the turbine shutdown.

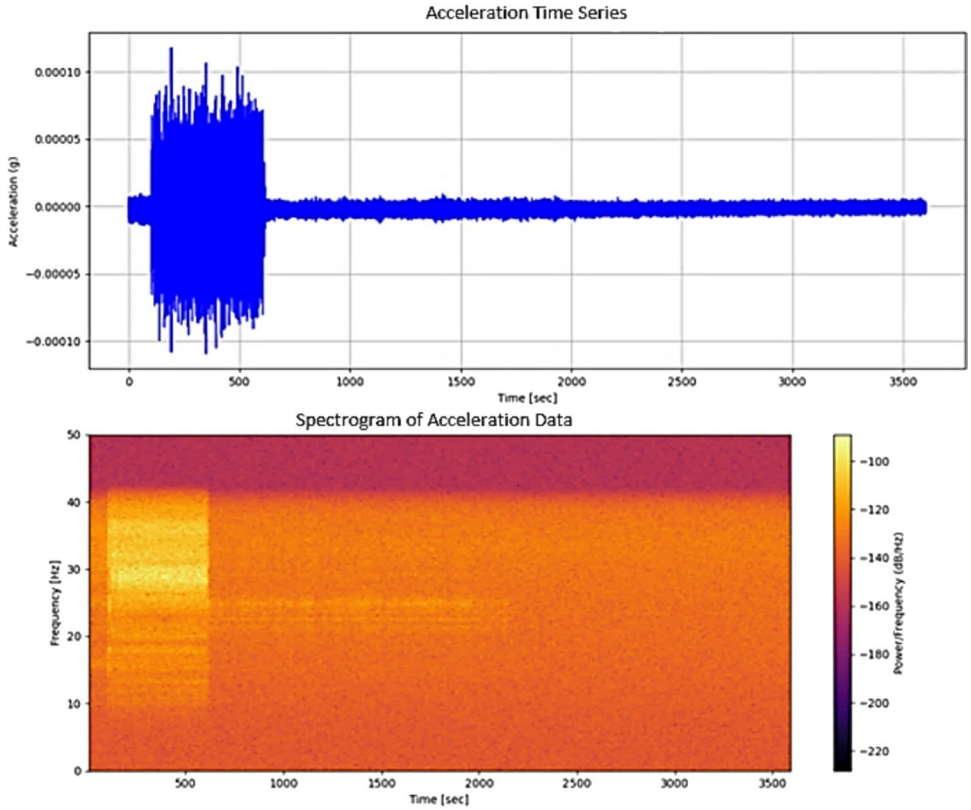


Fig. 4 Resonance condition after turbine shutdown

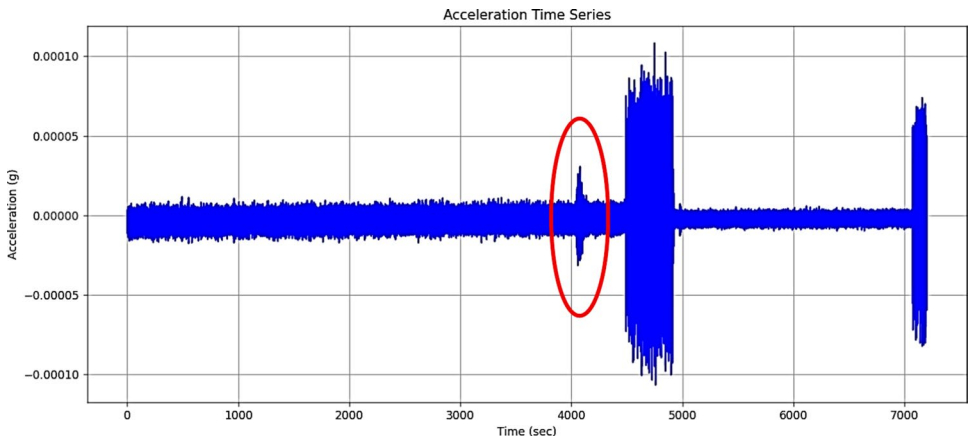


Fig. 5 Selçuklu earthquake (01.08.2023) acceleration time graph

These intervals highlight the dynamic changes in frequency and amplitude, providing insights into the interaction between natural seismic activity and artificial vibrations caused by turbine operation conditions.

Figure 6 presents the PSD graph for the dataset recorded during the earthquake. Analyzing the PSD graph reveals the following observations:

- During the turbine shutdown, most of the signal energy was concentrated at higher frequencies, particularly in the 29–30 Hz range.
- During the earthquake, the signal energy was predominantly concentrated at lower frequencies, within the 0–10 Hz range.
- Following the turbine's cessation, a prominent peak emerges around 25 Hz, suggesting a dominant frequency associated with the system's natural or resonant frequencies.

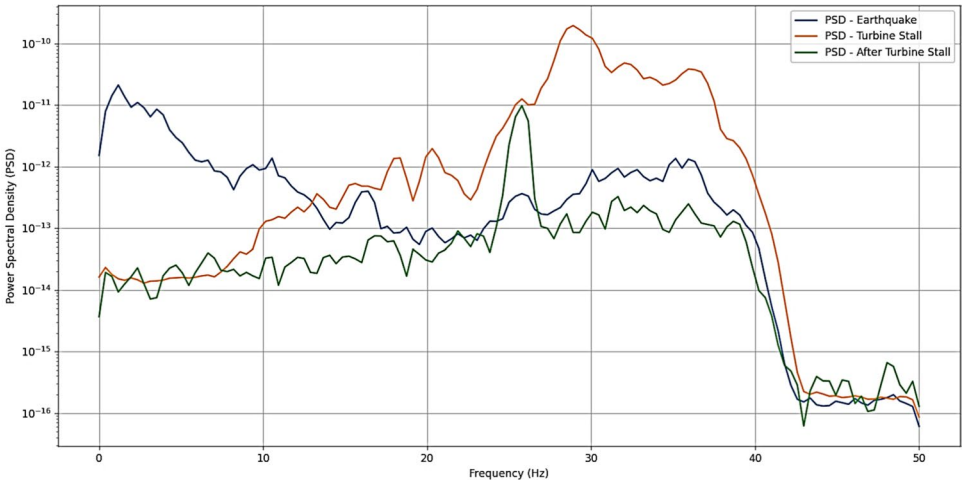


Fig. 6 Earthquake (01.08.2023) PSD graph

Table 2 Earthquake record (01.08.2023) spectral properties

Case	SC (Hz)	SB (Hz)	SRF (Hz)	PPF (Hz)	BAE
Earthquake	7.25	10.26	4.68	1.17	3.26E-12
Turbine Stall	30.46	3.17	31.25	28.90	9.57E-11
After Turbine Stall	26.16	4.48	26.17	25.78	2.28E-12

These findings demonstrated the distinct frequency behaviors under different conditions, emphasizing how seismic and artificial sources affect the energy distribution in the frequency domain.

In Table 2, spectral features such as Spectral Centroid (SC), Spectral Bandwidth (SB), Spectral Roll Off Frequency (SRF), Peak PSD Frequency (PPF), and Bandwidth Average Energy (BAE) were calculated. When analyzed in conjunction with Fig. 2, it was evident that the sudden frequency spike following the turbine shutdown was concentrated around 25 Hz. These findings supported the hypothesis suggested during the spectrogram analysis phase: the frequency values persist for a short period immediately after the abrupt turbine shutdown.

In Fig. 7, the acceleration-time and PSD graphs of the earthquake dataset were analyzed. During the earthquake (7115 s), significant power was observed in the 0–7 Hz range, and the dominant energy was concentrated near 25 Hz. Since this earthquake occurred in a noise-free environment, where the turbine was inactive, the presence of the 25 Hz frequency supports the hypothesis that it corresponds to the natural frequency of the bedrock.

Based on these analyses, each feature's sensitivity and distinctiveness were evaluated for both operational states and earthquake events. Time-domain indicators effectively captured abrupt changes and impulsive behaviors, especially micro-scale vibrations that precede earthquakes and short-term effects caused by turbine activity. Spectral features revealed unique energy concentrations and frequency patterns that were not visible in the time domain. This provided a deeper understanding of the signal's spectral characteristics. Integrating both domains enabled the selection of physically meaningful and statistically distinctive features, enhancing the model's anomaly detection capabilities and improving its generalizability.

3.2 Feature extraction

Calculating features from different earthquakes and generalizing their relationships across all events is essential to establishing a non-time-series deep-learning prediction model. For this purpose, Principal Component Analysis (PCA) was conducted to determine the most meaningful spectral and statistical features across all earthquakes and identify the key features and combinations that best characterize them. PCA facilitates the analysis of critical

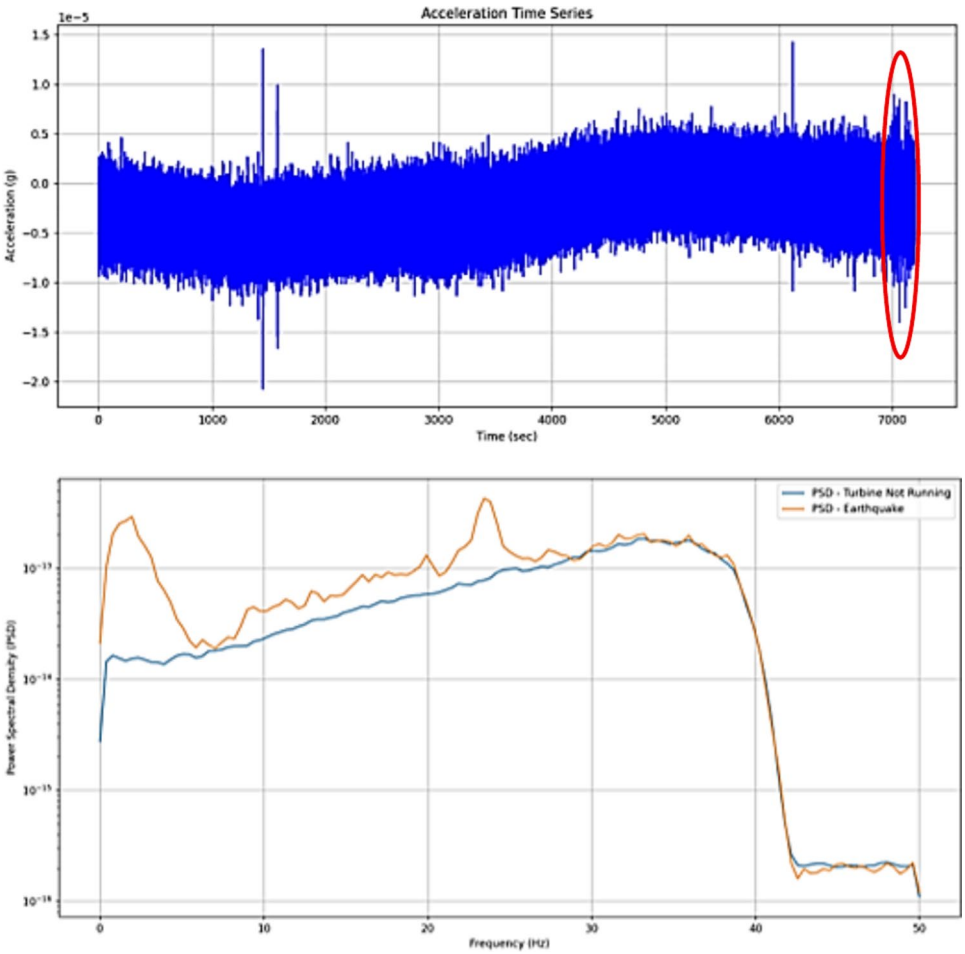


Fig. 7 Çorum earthquake (23.05.2024) acceleration time and PSD graph

underlying features in complex, high-dimensional datasets by identifying principal components that explain the maximum variance.

Key steps

Preprocessing of raw data

- Raw data obtained from various devices and in different formats were first converted into a unified.tdms format to ensure consistency throughout the analysis.
- Low-frequency drift and non-stationary components within the signal were eliminated by applying a detrending operation.
- Device-specific calibration coefficients were used to convert the raw data into the physical unit of acceleration (g), enabling meaningful interpretation.
- Signals from different sources were aligned on a common time axis through synchronization procedures.
- Synchronized signals were organized into separate columns, each representing an individual channel.
- The preprocessed data were exported in.csv format to facilitate subsequent analysis and visualization.

Feature identification and dimensionality reduction

- Spectral and statistical features that yielded the most significant results were selected.
- PCA was applied to reduce the complexity of the data while preserving the variance representing critical earthquake characteristics.

Pre-earthquake anomaly detection

- PCA transformed features were analyzed 1000–1500 s before each event in fixed time windows to evaluate the detectability of chaotic conditions before an earthquake.
- Changes in these features were monitored to identify patterns indicating potential pre-earthquake signals.

Anomaly detection using local outlier factor (LOF)

- The LOF algorithm was employed to detect outliers in the data.
- LOF calculates anomaly scores by comparing the density of each data point with its neighbors, highlighting points with significant deviations.
- This method was used to flag unusual patterns in the pre-earthquake data, providing insights into the chaotic conditions before seismic events.
- The accuracy of the LOF in detecting outliers was evaluated by observing whether outliers that could not be clustered with SOM (Self-Organizing Map) before applying LOF disappeared after its application. Following the removal of outliers identified by LOF from the raw data and reapplying SOM analysis, a reduction in outliers and an improvement in clustering performance were observed.

Expected outcomes

- PCA Analysis: Identification of the most critical features and their combinations for earthquake characterization, enabling efficient generalization across multiple events.
- LOF Anomaly Detection: Reliable detection of pre-earthquake patterns based on deviations in feature patterns, providing a foundation for constructing a robust non-time-series deep learning model for earthquake prediction.

As shown in Fig. 8, the process begins with ingesting raw data and proceeds by selecting a test file, while the remaining files are allocated for training. Both training and test data are subjected to windowing, followed by extracting spectral and time-domain features for each window. Based on these features, Local Outlier Factor (LOF) scores are calculated per window, and input–output pairs are generated for model learning. While windows from the training files are used to train the model, predictions made on the windows from the test file are used to evaluate the model's performance. This pipeline offers a robust and modular framework for real-time anomaly detection and prediction of earthquake-like events.

3.2.1 Principal component analysis (PCA)

PCA analysis was conducted for all earthquakes using the following spectral and statistical features: Spectral Centroid (SC), Spectral Flatness (SF), Spectral Slope (SS), Spectral Entropy (SE), Spectral Bandwidth (SB), Spectral Kurtosis (SK), Peak PSD Frequency (PPF), Spectral Roll Off Frequency (SRF), Energy (E), Peak PSD Energy (PPE), Crest Factor (CF), Skewness (S), Kurtosis (K), Bandwidth Average Energy (BAE), Frequency Band Energy Ratio (Low-Frequency Energy/High-Frequency Energy) (FBER), and others.

Key steps

PCA 1 and dominant features

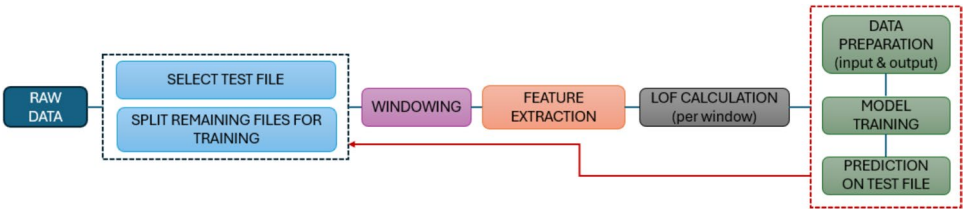


Fig. 8 Data flow diagram for LOF-based LSTM modeling

Table 3 PCA first component top 10 features

Earthquake	PCA 1 Top feature										
	%	1.	2.	3.	4.	5.	6.	7.	8.	9.	10.
1	76	SS	SF	BAE	PPE	SC	SB	E	K	SE	SK
		0.2845	0.2838	−0.2830	−0.2823	0.2818	0.2793	−0.2747	−0.2729	0.2719	0.2962
2	69	SC	SS	SB	FBER	BAE	WE	E	SF	SK	PPE
		0.3106	0.3103	−0.3079	−0.3050	0.3041	−0.2874	−0.2833	0.2829	0.2802	−0.2695
3	60	FBER	SS	SC	SK	E	PPE	SE	SF	SB	SRF
		0.3175	−0.3167	−0.3087	0.3025	0.2968	0.2894	−0.2863	−0.2816	0.2702	−0.2606
4	59	SE	E	PPE	SF	SS	SC	BAE	SRF	SB	FBER
		0.3184	−0.3140	−0.3130	0.3099	0.3087	0.3003	−0.2944	0.2877	0.2697	−0.2550
5	57	SS	E	FBER	PPE	SRF	SE	SC	SK	SF	PPF
		0.3254	−0.3251	−0.3232	−0.3211	0.3126	0.3121	0.2994	−0.2992	0.2745	0.2394

Table 4 Feature combinations with directions

EQ	PCA 1 Top Features									
	1	2	3	4	5	6	7	8	9	10
1	WE	SF	SB	PPE	SS	FBER	E	S	BAE	SC
2	SC	SS	SB	FBER	BAE	WE	E	SF	SK	PPE
3	E	SF	SS	PPE	BAE	WE	SRF	SC	SB	SE
4	SS	E	FBER	PPE	SRF	SE	SC	SK	SF	PPF
5	SS	SE	PPE	FBER	SF	E	BAE	SC	SRF	SB
6	FBER	SS	SC	SK	E	PPE	SE	SF	SB	SRF
7	SF	SC	SRF	PPF	SE	S	K	SB	PPE	E
8	FBER	SS	SC	PPE	SB	E	SK	PPF	SRF	BAE
9	SB	SC	FBER	SS	BAE	E	S	SK	WE	K
10	SE	PPE	SS	FBER	SRF	SF	SC	SK	BAE	E

- For each earthquake, the first principal component (PCA 1) was identified as representing most of the variance across the features.
- The top 10 features contributing most significantly to PCA 1 were calculated for all earthquakes. For five representative earthquakes, these features and their variance coefficients were presented in Table 3.
- Feature combinations with directions (Red: Negative, Blue: Positive) were provided for 10 representative earthquakes in Table 4. Additionally, Fig. 9 presents the most frequent feature combinations across earthquakes. Positive high values indicate a strong positive directional relationship between the feature and PCA 1, while negative high values show a strong but inverse relationship.
- The consistent appearance of specific features with high loading in the first PCA-1 across all earthquake cases, as shown in Fig. 10, suggests that these features are strong candidates for representing the underlying and generalizable characteristics of seismic events.
- Although certain features frequently emerge in both earthquake events and other types of occurrences, none of these features individually provides a directly distinctive criterion. As shown in Fig. 11, the recurrence of the same features across different scenarios indicates that feature-based discrimination is inherently limited when considered in isolation.

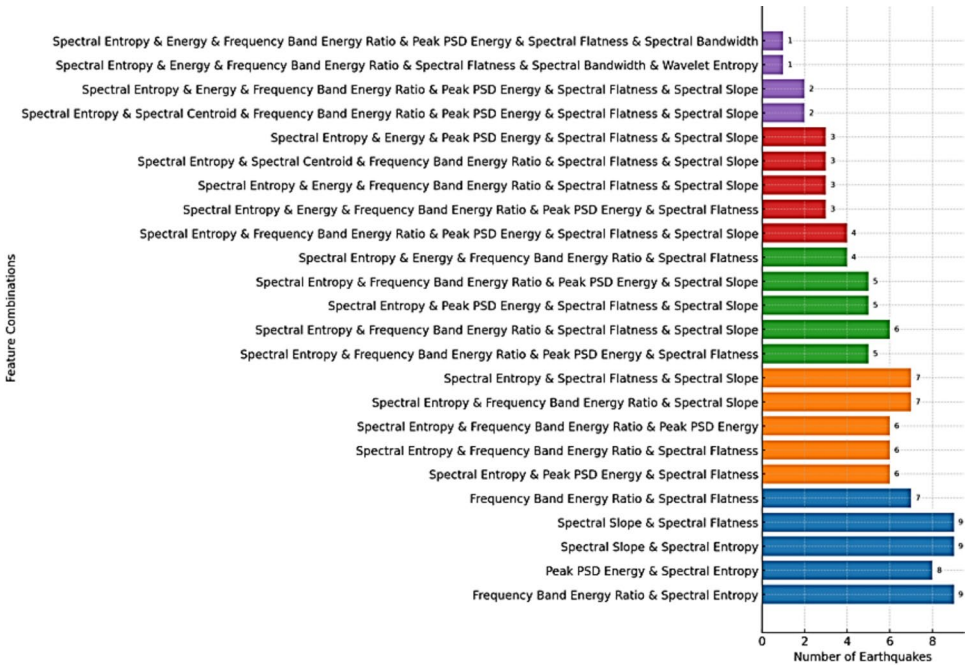


Fig. 9 Most frequent feature combinations across earthquakes

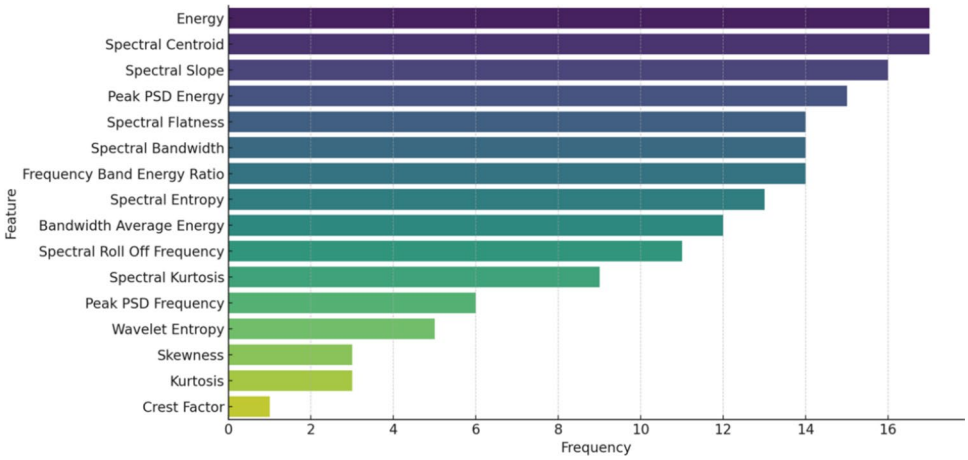


Fig. 10 Most frequent features in PCA-1: across earthquake cases

Patterns and variability

- It has been understood that PCA 1 components detect earthquakes with high percentage accuracy.
- In some cases, combinations of features contributed with similar weights, suggesting that the relative directional relationships among features, rather than individual features alone, are critical to distinguishing earthquakes.

Key insight

- The primary distinguishing characteristic of each earthquake was not a single dominant feature but rather the combination of multiple features and their directional relationships within the PCA 1.
- This provides a better understanding of earthquake characterization by underlining the importance of feature relationships in representing and distinguishing seismic events.
- The correlations among the direction and magnitude of characteristics and their combinations were considered significant. Based on the frequency of occurrences, a generalized conclusion was drawn for combinations that appeared six or fewer times across all earthquakes.

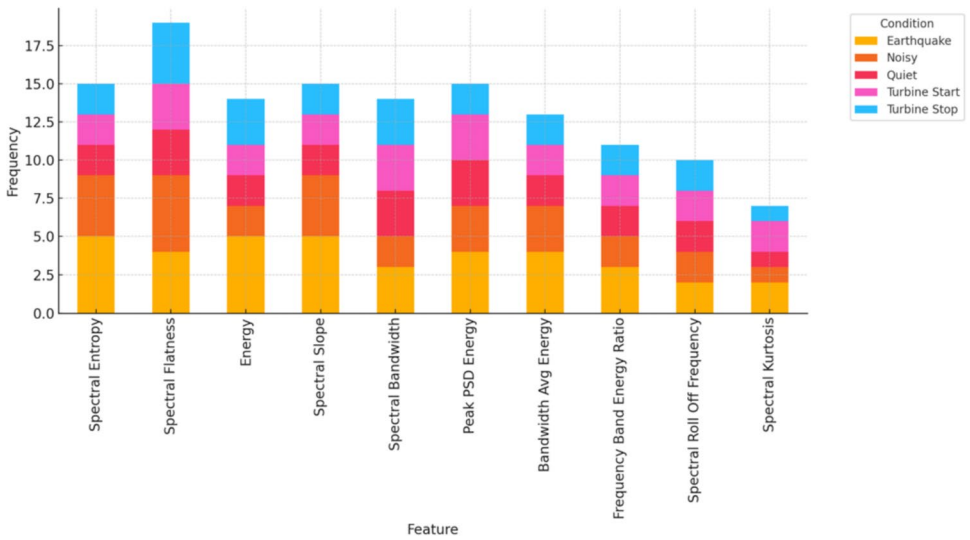


Fig. 11 Spectral feature in top 10 PCA by scenario

Implications

- By exploring feature combinations and their weights in PCA 1, it became possible to identify unique feature combination signatures for each earthquake.
- This insight is crucial for creating models that relate to earthquakes through various feature relationships, thus improving prediction accuracy and anomaly detection.

3.2.2 Local outlier factor analysis

Outlier detection using the LOF algorithm identifies patterns in a data point by analyzing its deviation relative to its surrounding data. The SOM method was applied to evaluate LOF results. Based on artificial neural networks, SOM clusters data by reducing it to a low-dimensional map, preserving its structure and patterns.

Silhouette Score and Best Davies-Bouldin Score metrics assessed clustering performance after SOM. As part of the study, LOF analysis was performed on raw pre-earthquake data to identify patterns before the earthquake. Outliers identified by LOF were removed from the raw data, and the SOM clustering performance was compared with the pre-LOF state to evaluate the methods effectiveness. The increase in the Silhouette Score indicates improved separation between clusters and augmented cluster consistency. The decrease in the Davies-Bouldin Score reflects more prominent inter-cluster differentiation.

Seismic signals are inherently nonlinear, noisy, and complex. They also exhibit time-varying statistical properties, which can reduce the effectiveness of traditional anomaly detection methods. For example, the Elliptic Envelope algorithm assumes that the data follow a multivariate normal distribution. Similarly, the One-Class SVM presumes that a hyperplane can separate normal and anomalous data using linear or kernel-based boundaries. However, real-world seismic data often deviate significantly from these assumptions, displaying chaotic behavior and high levels of noise [27, 28].

One significant advantage of the LOF algorithm is that it does not rely on any assumptions about data distribution. LOF uses a non-parametric approach that evaluates local density by analyzing the geometric relationships between neighboring data points. This makes it particularly suitable for seismic anomaly detection, where signals often contain statistically distinct, isolated, and nonlinear peaks. As a result, LOF performs well in signal windows with high variance or abrupt density changes, enabling the detection of complex seismic events.

These improvements demonstrate that LOF effectively identifies outliers, validating its application. In Fig. 12, an analysis of the acceleration-time graph revealed that the most significant anomaly related to the earthquake around 4062 s was observed approximately at 3593 s.

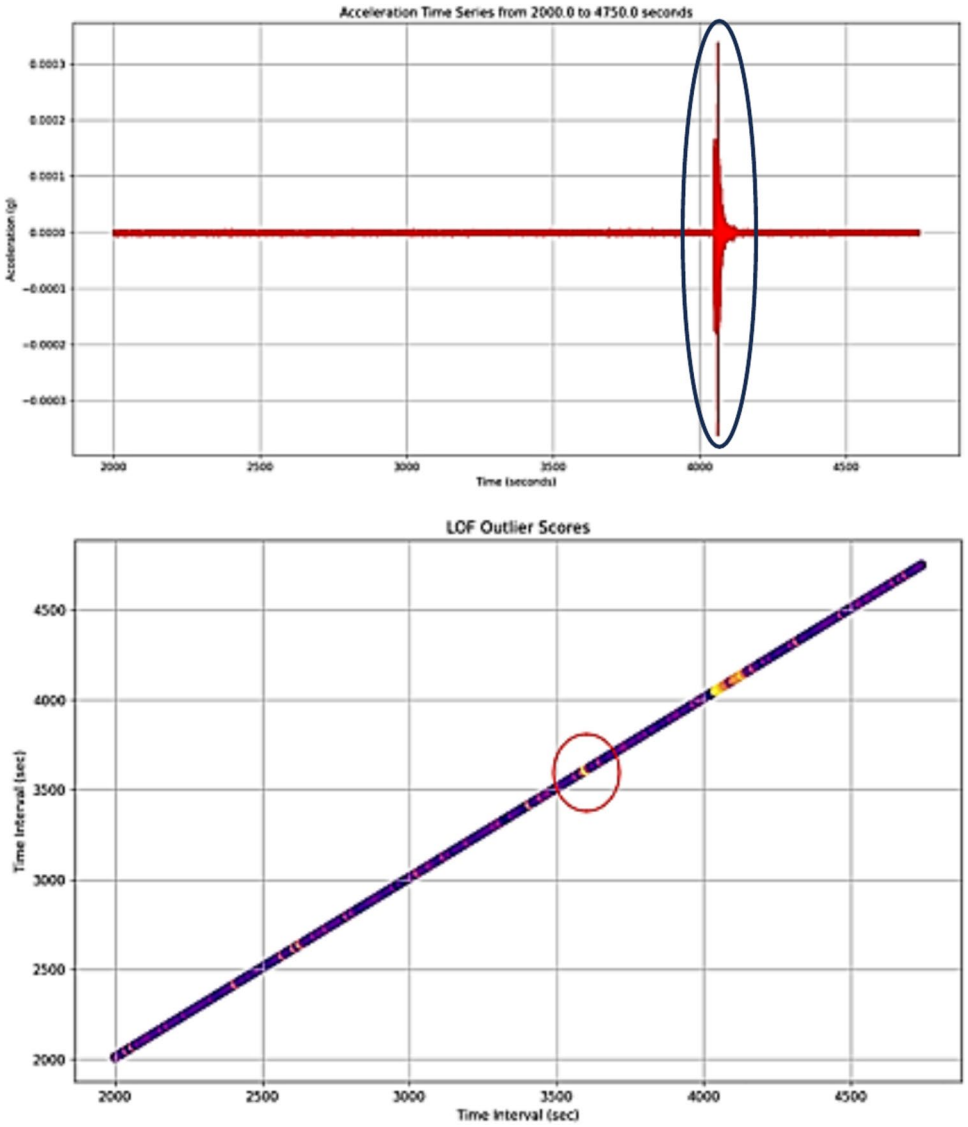


Fig. 12 Bolu earthquake record (14.10.2023) LOF score variation

In Fig. 13, the most significant anomaly associated with the earthquake between 6187 and 6229 s was detected approximately at 5029 s.

In Fig. 14, the most remarkable anomaly associated with the earthquake between 4915 and 4937 s was observed approximately at 4515 s.

It was concluded that applying the LOF algorithm effectively identifies patterns in sequential datasets, and the LOF score can be integrated into the developed LSTM deep learning model.

This study did not use the LOF as a traditional classification tool. Instead, it was treated as a target variable representing local density variations in the feature space. The model used spectral and temporal features from a given time window to predict the LOF score of the next window. This predictive approach combines LOF's sensitivity to local structural changes with temporal modeling, allowing for early detection of potential anomalies. In addition, the neighborhood size parameter in LOF was not fixed. Instead, it was dynamically adjusted based on the event type and the characteristics of each time window. This adaptive strategy increased the algorithm's sensitivity to local density variations and improved its ability to detect subtle anomalies more accurately.

Integrating LOF into a temporal prediction framework made the model more flexible in handling typical limitations, such as sensitivity to parameter settings and high-dimensional feature spaces. This approach allowed

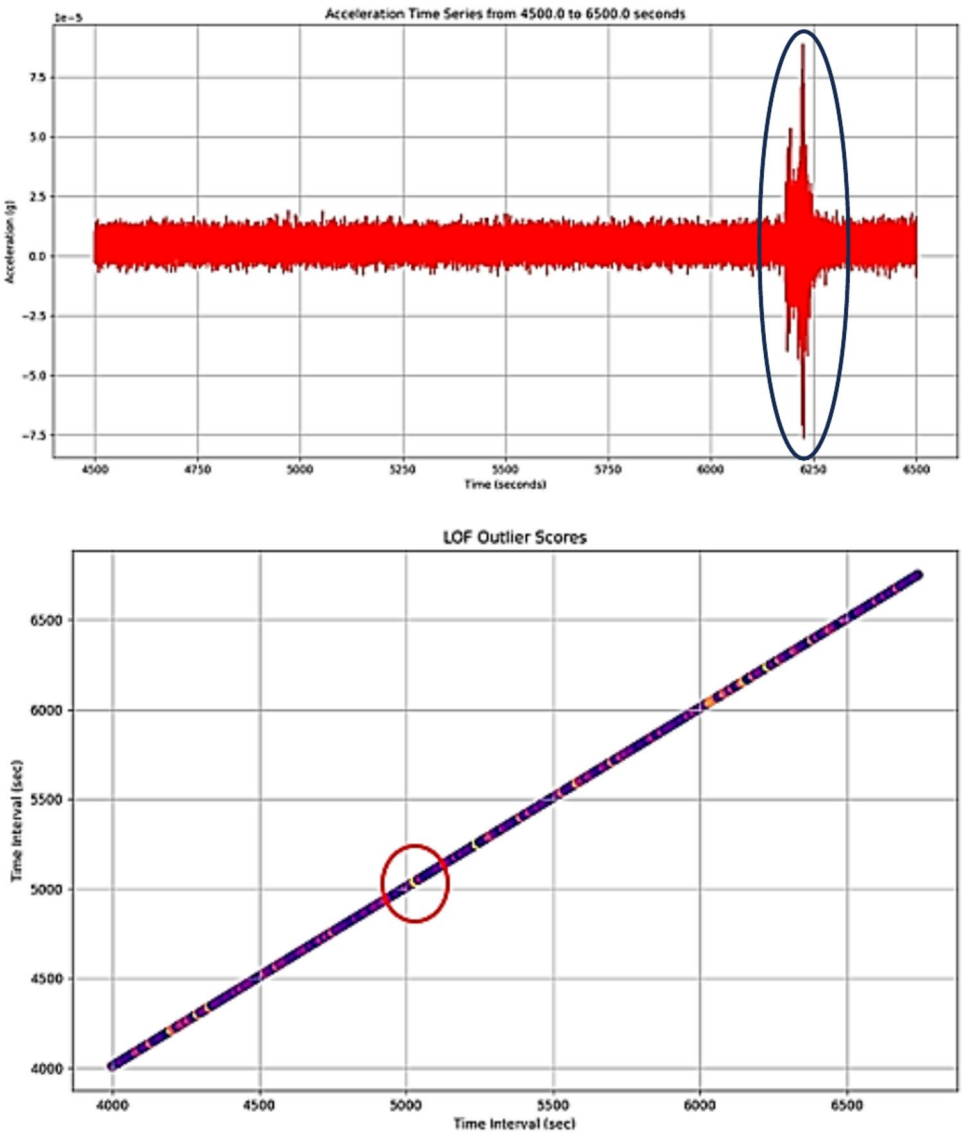


Fig. 13 Çanakkale earthquake record (04.03.2024) LOF score variation

the model to detect current anomalies based on past behavior and learn how local density patterns evolve, especially in seismic activity. As a result, the model achieved more accurate and interpretable representations of local anomaly patterns.

Similar to the comparative framework presented by [29], which evaluated multiple unsupervised anomaly detection algorithms for predictive maintenance applications, this study focuses on assessing the effectiveness of LOF, Isolation Forest (IF) and One-Class Support Vector Machine (OCSVM) for identifying operational and seismic anomalies in vibration data.

In Fig. 15, the raw acceleration time history displays distinct peaks corresponding to the turbine shutdown (at 1200 s), turbine startup (at 6100 s), and the earthquake event (at 4050 s) that occurred while the turbine was inactive.

In Fig. 16, the visualization presents the anomalies detected by the LOF method for the turbine shutdown, turbine startup, and the earthquake event defined in Fig. 15.

Since LOF compares the local density of each data point with that of its neighboring samples, it did not classify transient regime changes (such as turbine startup or shutdown) as anomalies, because these transitions exhibit similar statistical characteristics to their surrounding windows. Although the signal amplitude varies during these

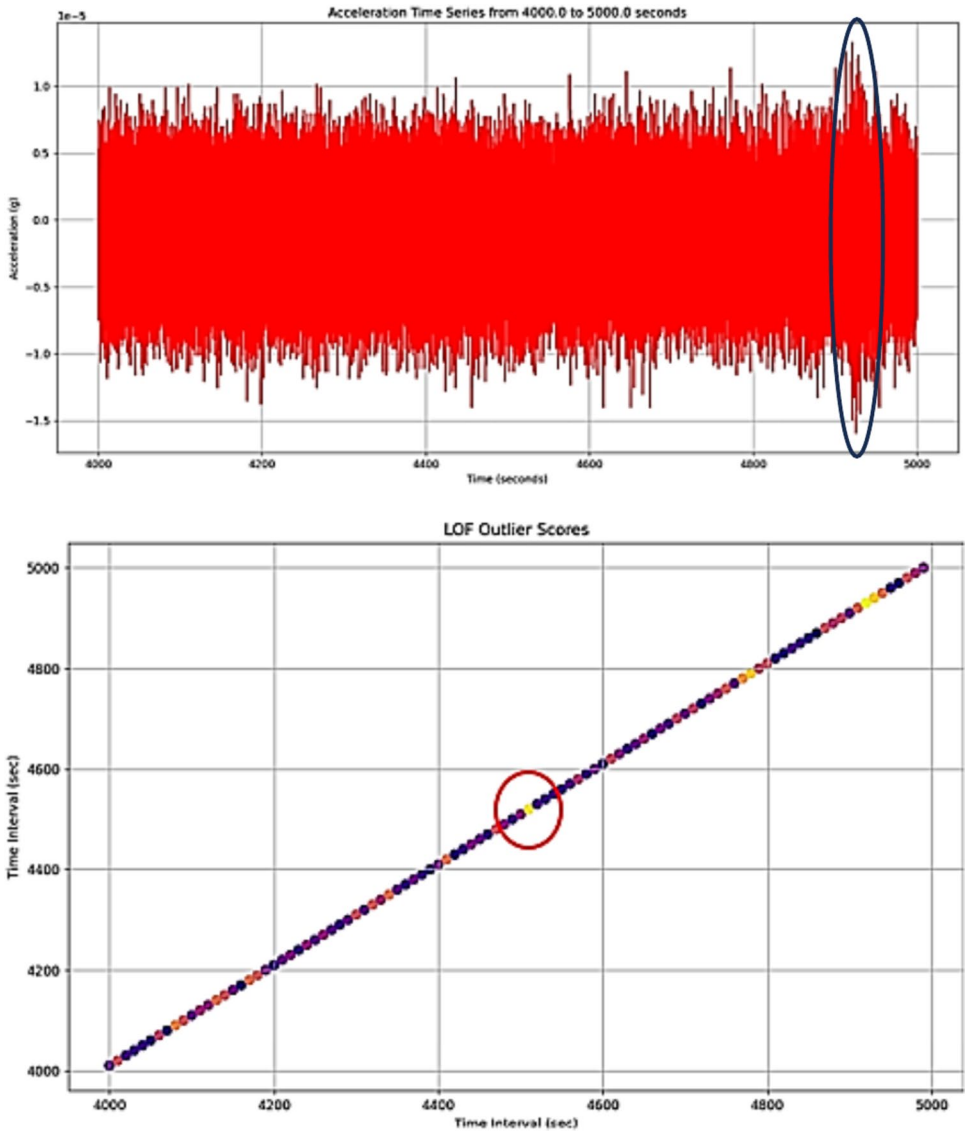


Fig. 14 Balıkesir earthquake record (21.03.2024) LOF score variation

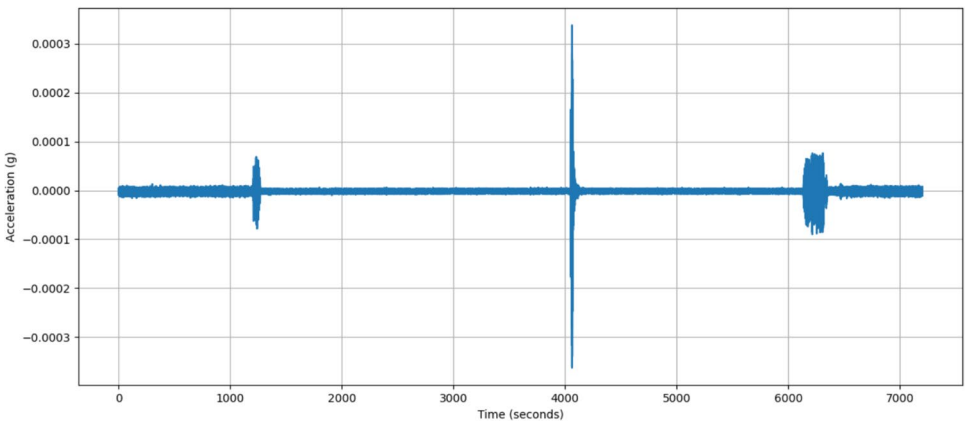


Fig. 15 Bolu earthquake record (14.10.2023) raw acceleration time graph

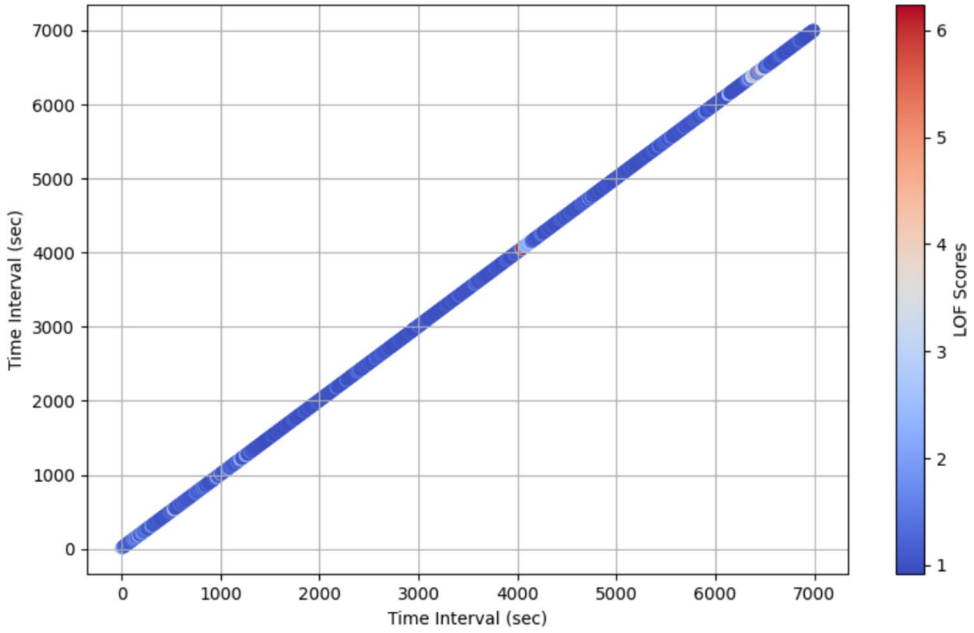


Fig. 16 Bolu earthquake Record (14.10.2023) LOF score variation

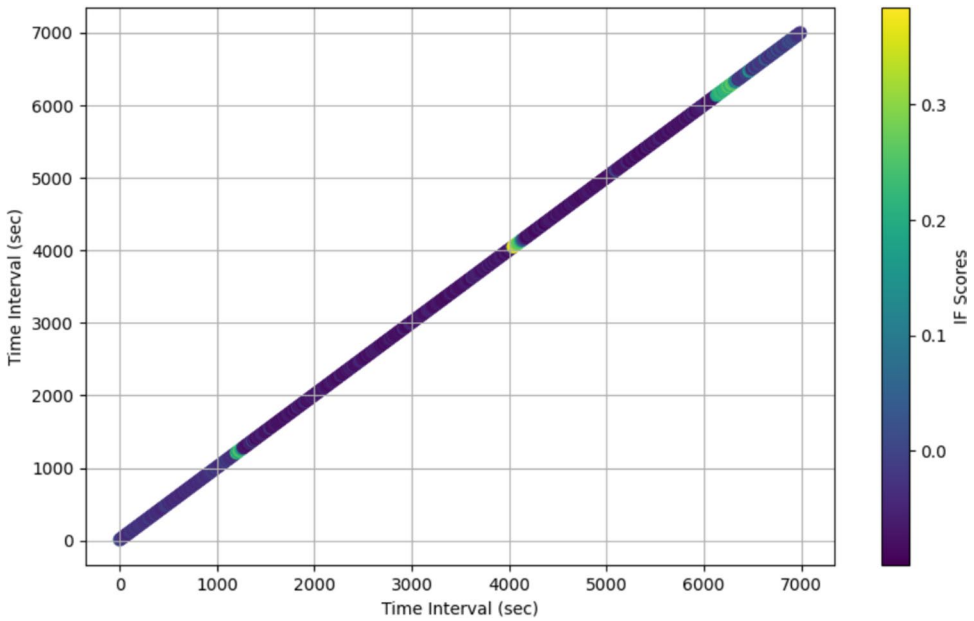


Fig. 17 Bolu earthquake record (14.10.2023) isolation forest score variation

operational transitions, the adjacent segments behave similarly; hence, the LOF method regarded these periods as locally consistent.

In contrast, during the earthquake event, the signal exhibited a distinct deviation from its surrounding segments in terms of both amplitude and spectral content, resulting in a local disruption of the density distribution. The LOF method identified the observations within this interval as significantly sparser compared to their neighbors and, therefore, classified only this region as anomalous.

In Fig. 17, the visualization presents the anomalies detected by the IF method for the turbine shutdown, turbine startup, and the earthquake event defined in Fig. 15.

The IF method responded strongly to regime transitions such as turbine shutdown and startup, where abrupt changes in amplitude, mean, variance, and spectral energy distribution occurred. These sudden statistical shifts

led to the formation of low-density regions in the feature space, causing the model to isolate the corresponding observations with fewer splits. As a result, the method misclassified these segments as anomalies, despite them representing normal operational transitions rather than genuine abnormal events.

In Fig. 18, the visualization presents a comparative analysis of the anomaly scores obtained from the LOF, IF, and OCSVM methods for the turbine shutdown, the earthquake event that occurred while the turbine was inactive, and the turbine startup defined in Fig. 15.

Since the LOF is a density-based method, it is capable of capturing small-scale statistical irregularities within the data. Accordingly, it identified the earthquake event as a region of significantly lower local density compared to its surroundings, while not classifying the turbine startup and shutdown transitions as anomalies. Furthermore, its sensitivity to minor fluctuations observed prior to the earthquake indicates that the system is responsive to potential precursor behaviors.

In contrast, the IF, which isolates anomalies by recursively partitioning the feature space and assigning higher anomaly scores to low-density regions, is sensitive to large-scale deviations in the data distribution but relatively insensitive to small-scale variations [30]. As a result, although it correctly identified the earthquake as an anomaly, it also interpreted the turbine startup and shutdown transitions as anomalies of comparable magnitude. Consequently, the method evaluated these regime transitions at a similar statistical significance level to the earthquake, failing to distinguish between the two types of events. Moreover, it exhibited almost no response to the subtle micro-changes observed prior to the earthquake.

The OCSVM, on the other hand, constructs a global decision boundary that encloses the majority of normal data within a high-dimensional space [31]. It is slightly more sensitive than IF to small fluctuations, however, because it models the normal domain with a single smooth boundary, it tends to evaluate the earthquake and turbine transitions with similar sensitivity. Despite exhibiting a consistent fluctuation pattern prior to the earthquake, this behavior did not generate sufficient contrast to distinctly separate the pre-earthquake period from the normal state.

3.3 Deep learning model

LSTM is a type of RNN designed to analyze time-series data and model temporal dependencies. RNNs process data sequentially and can retain information from previous time steps. Unlike traditional feedforward networks, they incorporate historical context into their computations. LSTM networks extend the capabilities of standard RNNs by using gating mechanisms. These gates regulate the flow of information, helping the model decide which

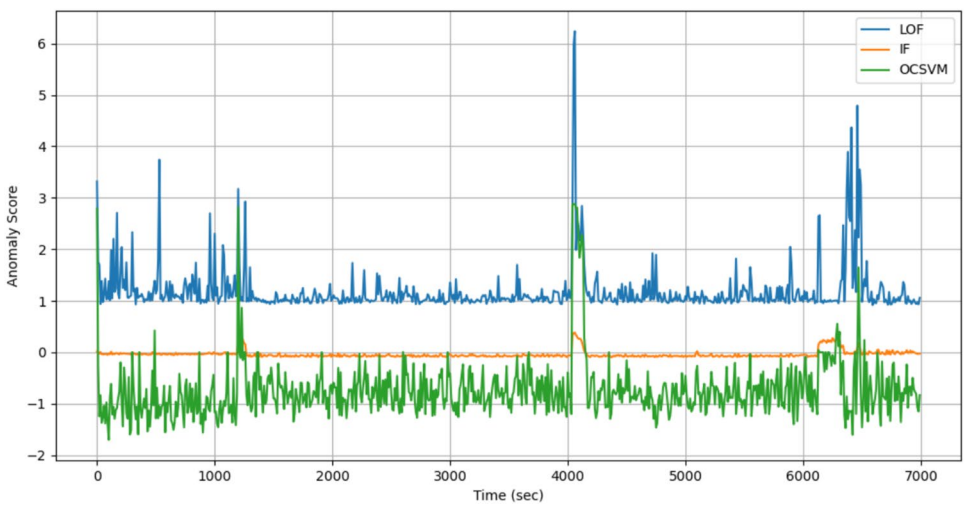


Fig. 18 Bolu earthquake record (14.10.2023) LOF, IF, OCSVM outlier scores comparison

data to retain and which to discard. This structure enables LSTM networks to manage long-term dependencies effectively and improves performance on tasks involving sequential patterns.

In this context, the earthquake dataset was divided into fixed-size windows, and spectral and time-domain features were calculated for each window. The main goal was to use the features from the current window to predict the LOF score of the next window using an LSTM model. The model was trained by minimizing a loss function, which measured the difference between the predicted LOF score and the actual LOF score calculated for the next window Fig. 19. This approach permitted the model to learn and improve its accuracy in identifying and predicting patterns in sequential earthquake data.

As a result of the PCA analysis performed for each earthquake, using the selected spectral and statistical features, it was recognized that the directions and combinations of these features were more informative than their magnitudes. The features calculated for each earthquake and its precursors were vectorized. The differences and similarities between these vectors and those calculated for neighboring windows were assessed directionally using the LOF value. In this context, the Cosine Similarity algorithm has been employed as a similarity metric to quantitatively assess the directional alignment and proximity between vector representations, providing a robust measure for evaluating the degree of similarity.

After confirming that the LOF score, calculated from the selected features, could successfully detect patterns, the LSTM model was trained using the features from preceding time windows to predict the LOF scores of subsequent ones. In this approach, the spectral and statistical features from 20 previous windows (5 s) were used as inputs to predict the LOF score of the subsequent window as the output. The aim was to determine whether the selected features could be used to predict earthquake-related patterns in advance.

The LOF score for a given window was calculated by considering its anomaly relative to the nearest 20 windows. The actual LOF score of the predicted window was computed, and the Mean Square Error (MSE) between the expected and actual LOF scores was used as the loss function. MSE, a standard optimization algorithm in deep learning for gradient descent, updates the model weights step by step to minimize the loss function. MSE is more sensitive to significant patterns because it amplifies larger errors. This amplification effect enhances the model's sensitivity to anomaly deviations, helping achieve more accurate detections within the dataset.

The established LSTM model employs a two-layer, Bidirectional LSTM architecture to analyze sequential information in time-series data in both forward and backward directions. Increasing the number of layers while reducing the number of neurons in subsequent layers is a common strategy to balance model complexity and computational cost.

Model architecture details

First layer

- 150 neurons were consistent with the SeLU activation function applied to each unit for stability and balance.
- The Return Sequences parameter was set to True, allowing the output to pass as a sequence to the next layer.

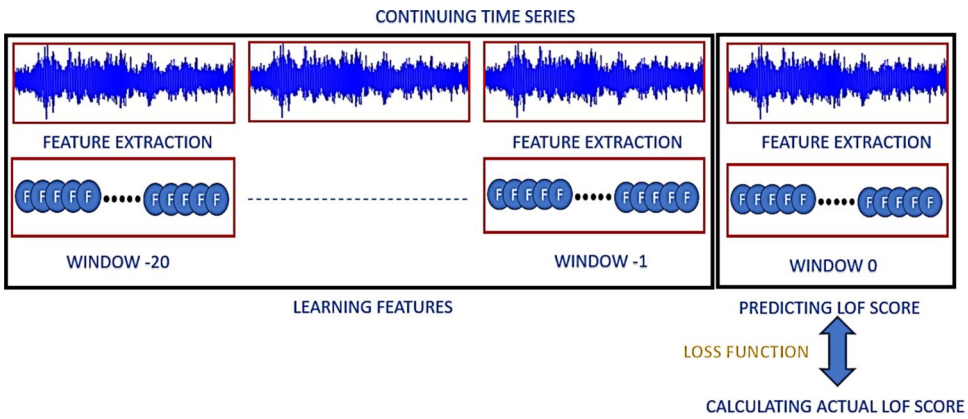


Fig. 19 Established LSTM learning and prediction model

- A Dropout Layer with a 20% rate was added to deactivate neurons, reducing the risk of overfitting randomly.

Second layer

- A bidirectional LSTM layer with 100 neurons, using the SeLU activation function to maintain balanced outputs.
- The Return Sequences parameter was set to False, producing only the output of the last step to focus solely on the prediction.

Output layer

- A Dense Layer with a single unit outputs the predicted value, specifically the LOF score for the next window.

Optimization and loss function

- The model used the Adamax optimizer, known for its stability and efficiency in large datasets.
- The MSE was employed as the loss function, commonly used in regression problems like time-series prediction, amplifying more significant errors to improve sensitivity.

Hyperparameter optimization

Hyperparameter optimization was performed to achieve optimal model performance:

- The number of layers, neurons, and different activation functions.
- Learning rate and optimizer type.
- Sampling window sizes were used in the Fast Fourier Transform FFT process for spectral feature extraction.
- The number of neighboring points considered for LOF computation.
- Both sliding and fixed window types.

The configuration with the lowest loss function value was selected, ensuring a balance between capturing patterns in the data and applying LOF optimally with an ideal number of neighbors.

Selecting an earthquake record that captures and embodies the most complex and variable real-world conditions is critical for effective hyperparameter optimization. The Balıkesir Earthquake Record (dated 21.03.2024) was chosen to meet this requirement. This event occurred in a noisy operational environment, immediately following turbine activation, offering high signal diversity and structural complexity. The Parallel Coordinates Plot Fig. 20 was employed to analyze the impact of different hyperparameter combinations on model performance. In this plot, each line represents a distinct model trial.

The objective is to identify the hyperparameter combination that yields the lowest training and validation loss values while minimizing the difference between them. According to this criterion, the combination highlighted in light green was selected for the LSTM model. This combination resulted in low error rates and minimized the gap between training and validation losses, thereby achieving a model with high generalization capability.

Training and testing

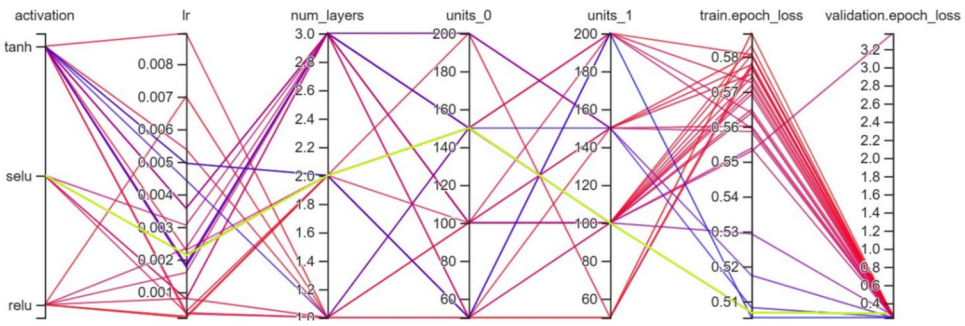


Fig. 20 Effect of LSTM hyperparameter combinations on training and validation loss

- The model was trained incrementally, continuously updating weights for all earthquakes and using cross-validation to generalize effectively.
- It was tested on previously unseen test data to predict the LOF score for the next window based on current window features.
- The goal was to identify patterns associated with earthquakes and precursors.

Overfitting prevention

- Cross-validation and testing on unseen data minimized overfitting risks.
- Incremental updates across all earthquakes ensured robust learning applicable to varied seismic patterns.

Outcome

The LSTM model optimizes computational complexity and performance for sequential anomaly detection and time series analysis. Effectively capturing important patterns in spectral features ensures accurate estimation of LOF scores for the following time windows. Optimized parameter combinations ensure the method's robustness and reliability.

- Smaller numbers of neighbors for LOF and more oversized spectral windows in Fourier transforms appear to be the most effective combinations for reducing training loss.
- A reduced number of neighbors in the LOF method, combined with more expansive spectral windows in Fourier transforms, has been identified as the optimal configuration for reducing training loss.
- However, using large window sizes for calculating spectral and statistical features negatively impacts model performance. This indicates that selecting an appropriate window size is critical for practical analysis.

When comparing the performance of models used for time series-based anomaly detection, the LSTM-based model produced more stable and reliable results than the CNN-based model. This superiority is attributed to several key factors: the LSTM model's ability to identify early signs of anomalies before their onset, its adaptability in returning to typical behavior following an anomalous event, and its consistently accurate predictions under low-noise conditions, as illustrated in Fig. 21**.** While the current study focuses on the comparison with CNN architectures, future research will incorporate comprehensive benchmarking against plain LSTM and feedforward neural network (FFNN) architectures to further validate and generalize the proposed model's performance.

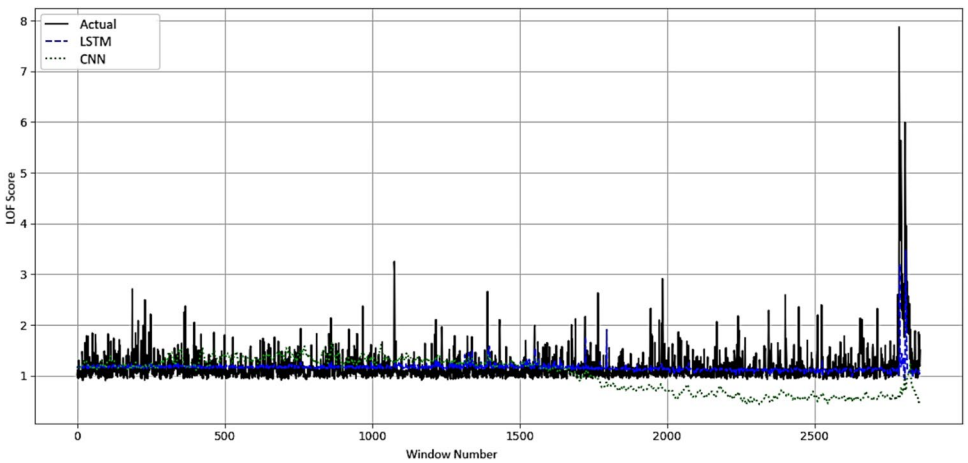


Fig. 21 Akdeniz earthquake record: comparison of anomaly with CNN

4 Results

Analysis of Fig. 22 revealed the anomaly associated with the seismic event at 5083 s. However, the actual patterns that emerged following the earthquake were not detected.

Analysis of Fig. 23 indicated that the anomaly associated with the earthquake event around 6250 s was detected, similar to the findings in Fig. 22. However, actual patterns unrelated to seismic events, observed in the 390th and 170th windows, were not predicted.

Figure 24 presents the acceleration-time graph and the predictive results, accurately capturing the anomaly during the earthquake between approximately 6416 and 6499 s.

Analysis of Fig. 25 revealed that the seismic event occurring between approximately 4916 and 4999 s, which was obscured in the acceleration-time graph by turbine operational noise, was successfully predicted. Furthermore, as reported in previous cases, the predictions did not include patterns unrelated to seismic events.

The seismic event that occurred near 7000 s was accurately predicted in Fig. 26, despite being obscured by turbine-induced noise in the acceleration-time graph. Moreover, the system effectively distinguished and excluded non-seismic patterns, thereby preventing the false predictions observed in previous figures.

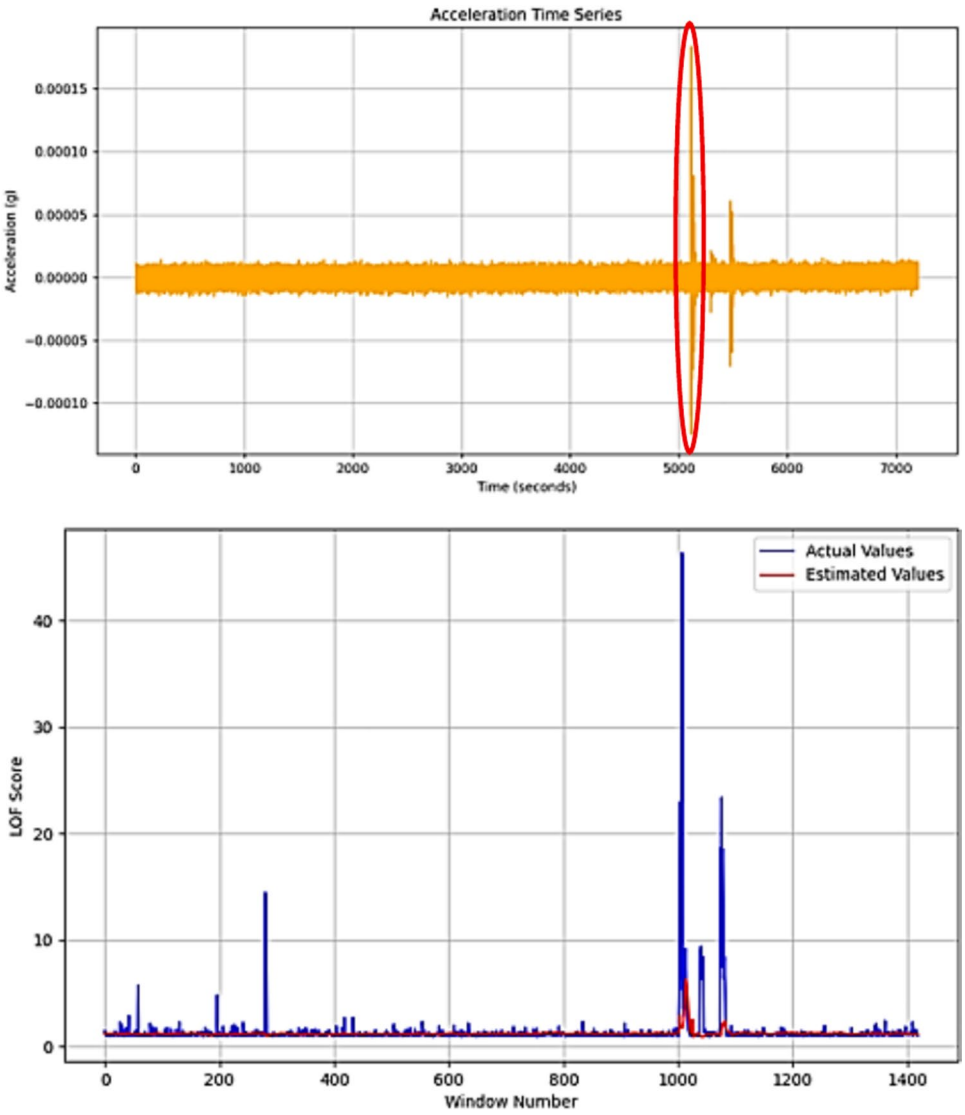


Fig. 22 Afyon earthquake record (11.07.2024): prediction of anomaly

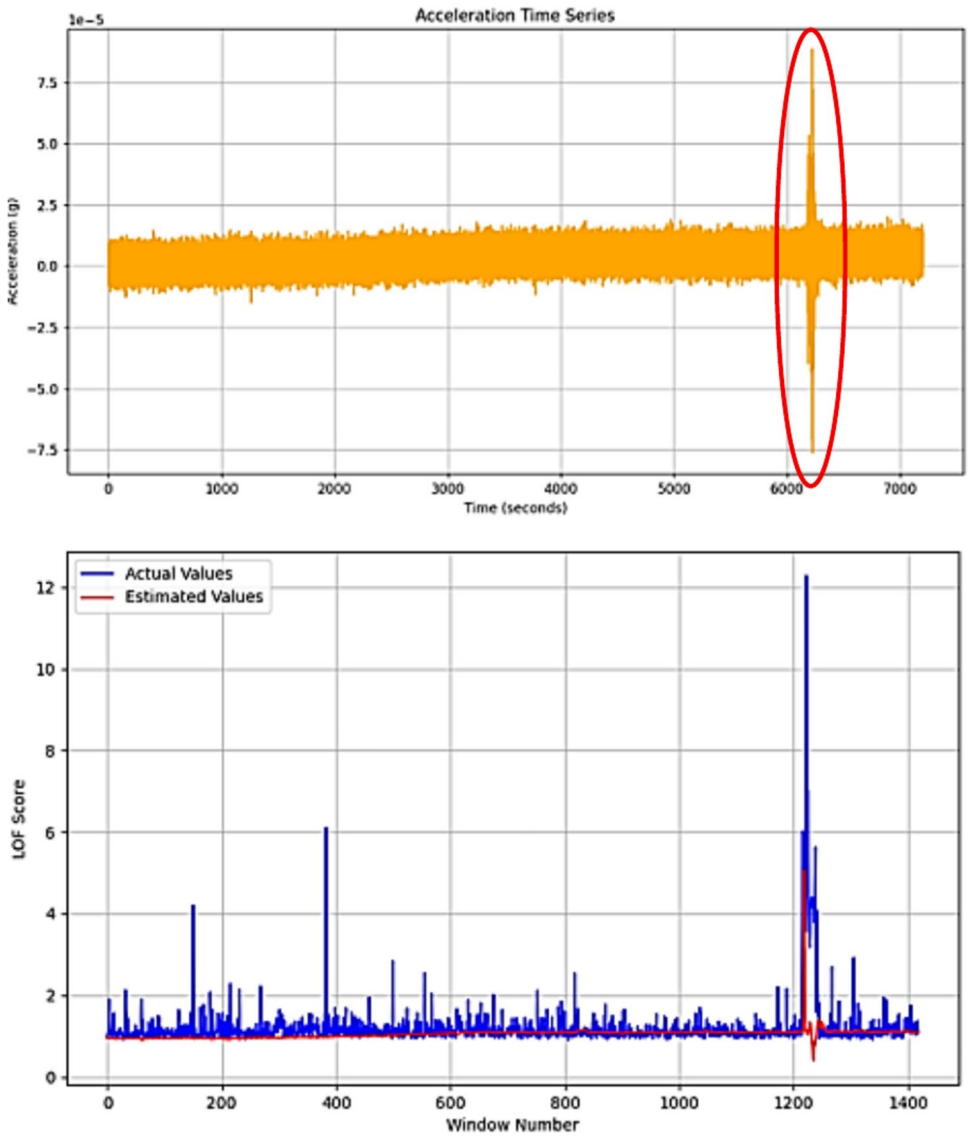


Fig. 23 Bursa earthquake record (04.12.2023): prediction of anomaly

Figure 27 displays the initiation of turbine operations between approximately 3545 and 3725 s, followed by an earthquake in a noisy environment around 4954 s. Analysis of the prediction results graph confirmed that the anomaly associated with the earthquake was accurately predicted.

The acceleration-time graph in Fig. 28 demonstrates the occurrence of an earthquake in a noisy environment at around 6030 s, followed by the initiation of turbine operation at approximately 7000 s. Furthermore, analysis of the prediction results graph indicated that the anomaly associated with the earthquake was accurately identified.

Although the seismic event was obscured in the acceleration-time graph due to turbine noise, it was successfully predicted between 6000 and 6180 s in Fig. 29. Consistent with previous figures, patterns not associated with seismic activity were effectively excluded from the predictions.

Analysis of Fig. 30 confirmed the prediction of the earthquake-related anomaly at 4083 s. The LOF score analysis also distinguished this seismic event from the turbine shutdown at 1318 s and the subsequent resumption of turbine operations between 6181 and 6363 s.

The assessment of Fig. 31, consistent with Figs. 20, 21, and 24, demonstrated that the earthquake occurring around 4217 s, which was obscured in the acceleration-time graph by turbine operation noise, was precisely predicted.

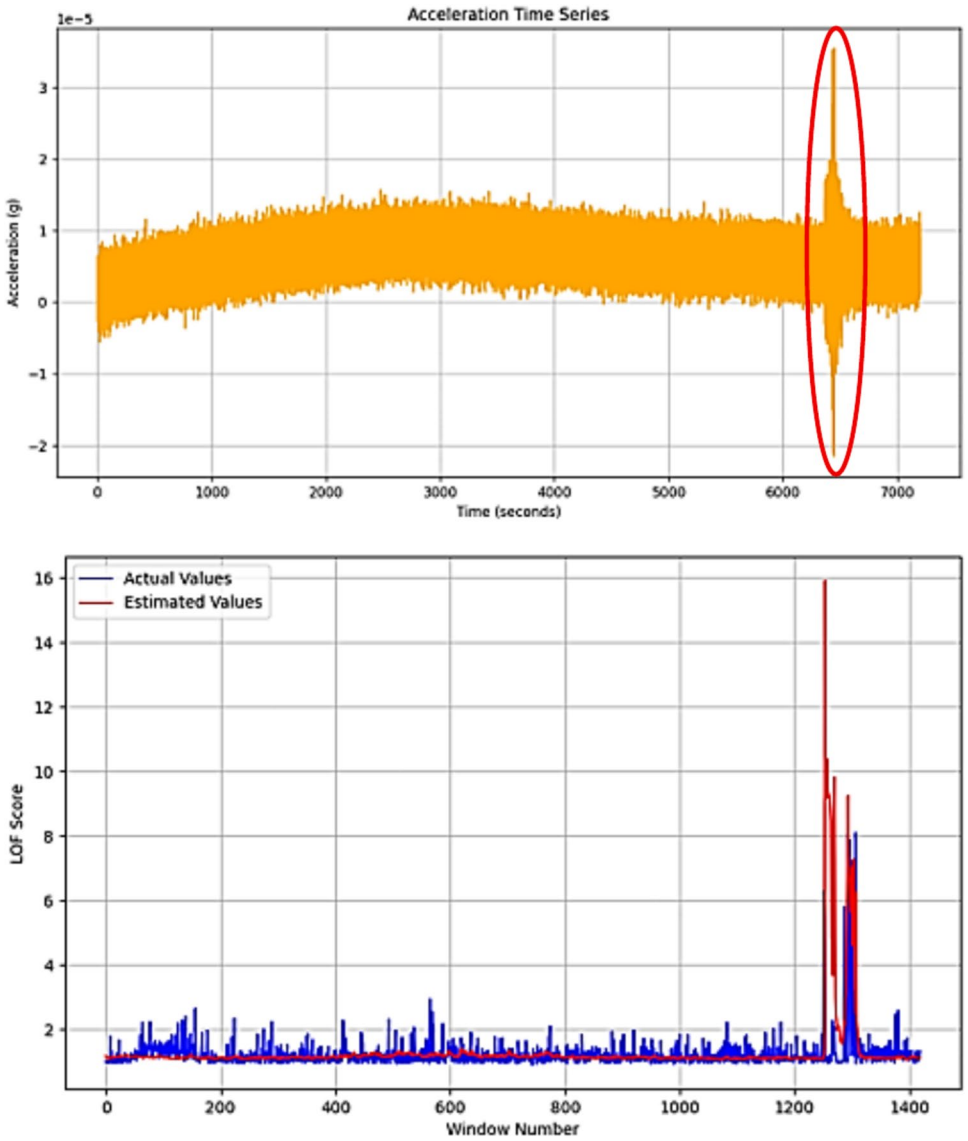


Fig. 24 Kozan earthquake record (25.07.2023): prediction of anomaly

Analysis of Fig. 32 revealed that the earthquake at 5900 s, which was obscured in the acceleration-time graph by turbine operation noise, was successfully identified, consistent with the findings in Figs. 24, 21, and 20. Moreover, patterns unrelated to seismic activity, including the anomaly associated with the turbine start-up peak at the beginning of the recording, were not predicted.

The seismic event occurring between 3900 and 4136 s, which was masked by turbine operational noise in the acceleration-time graph, was precisely predicted in Fig. 33.

Outcome

The results indicate that the model performs exceptionally well for moderate to large-magnitude earthquakes. For earthquakes with a magnitude of 4.5 and above, both high True Positive Score (TPS) and high Signal Similarity Detection Score (SSDS) values were achieved, along with low Mean Absolute Error (MAE) values. These results demonstrate the model's ability to learn and interpret the characteristic signal patterns of such earthquakes. As shown in Fig. 34, although relatively lower performance metrics were observed for smaller earthquakes in the 4.0–4.4 magnitude range, this reduction can be attributed to the less distinctive signal features of low-magnitude events and their greater similarity to background data.

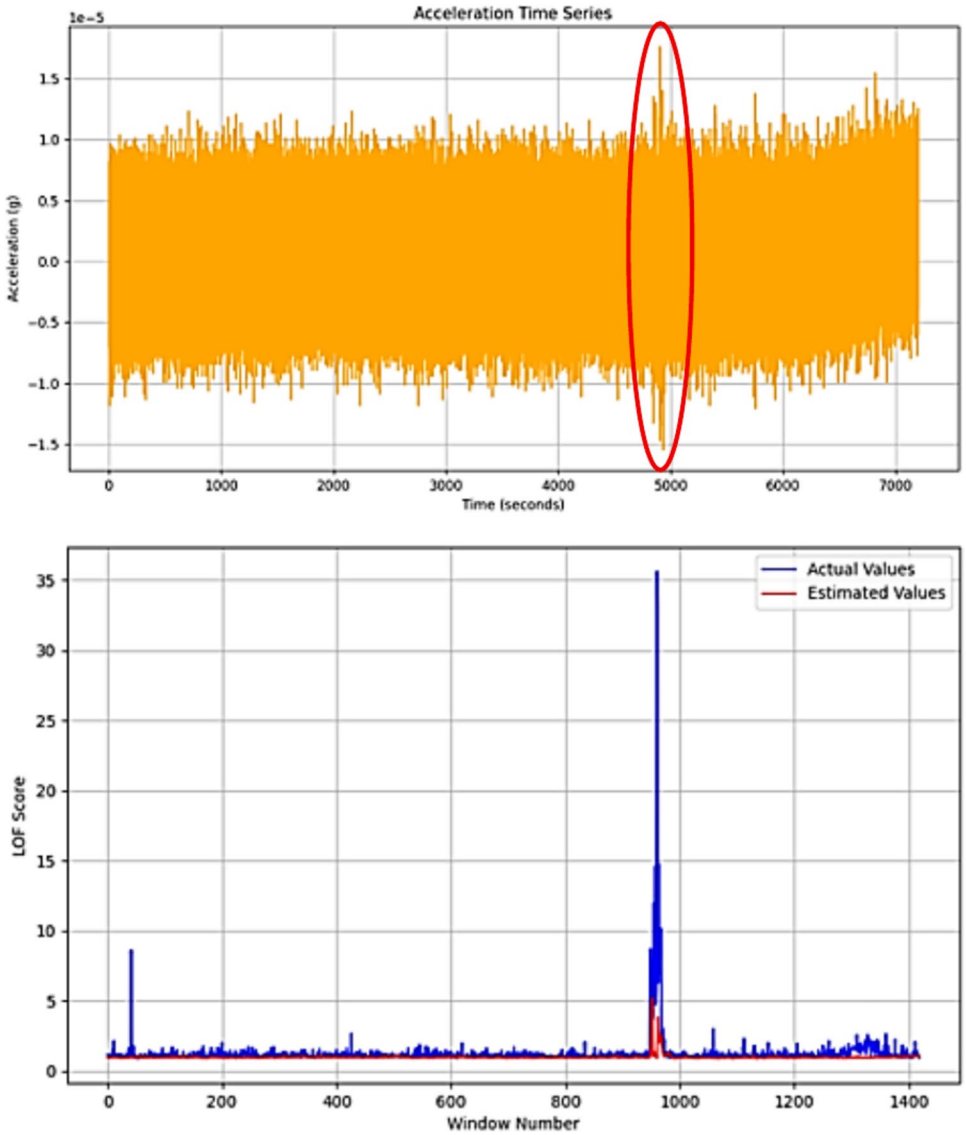


Fig. 25 İzmir earthquake record (27.01.2024): prediction of anomaly

As shown in Fig. 35, the relationship between model performance and physical parameters such as earthquake depth and epicentral distance was assessed using four key metrics: MAE, TPS, FPSR, and SSDS. The MAE exhibited a moderate negative correlation with depth and distance, indicating improved background prediction for deeper and more distant events. In contrast, TPS and SSDS displayed weak or negligible correlations, suggesting that peak detection and timing accuracy are relatively stable across varying physical conditions. The FPSR showed a slight increase with depth and a decrease with distance, reflecting minor sensitivity to noise in deeper events. While background error is influenced by depth and distance, the model's core detection and timing capabilities remain generalizable and robust.

Key findings

The model disregarded patterns except for earthquakes, even when those were visible in the acceleration-time graph. This result demonstrated the model's ability to accurately differentiate earthquakes from other events. Using spectral and statistical properties, the LSTM model could predict the peaks related to earthquakes that were not visible in the acceleration-time graph, even when the earthquake occurred in a noisy environment. In addition, the earthquake anomaly was successfully isolated from the abrupt patterns brought on by the start or stop of the turbine.

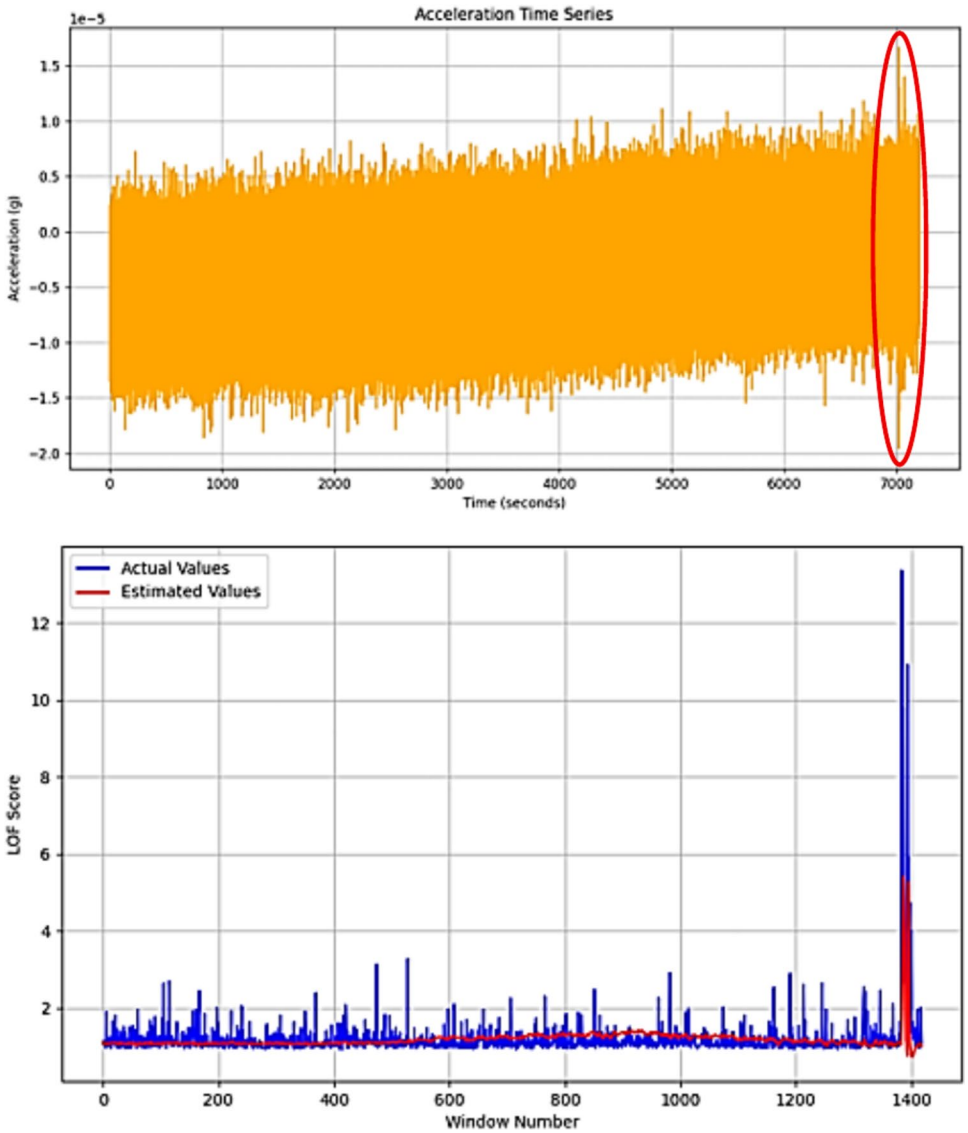


Fig. 26 Akdeniz earthquake record (10.03.2024): prediction of anomaly

5 Conclusion and discussion

This study demonstrated that surface vibrations related to far-focus earthquakes can be directly detected using acceleration time recordings from a strong ground motion recorder. However, identifying meaningful patterns in these records requires more than simply analyzing raw time-series signals. In this context, feature engineering plays a vital role in extracting informative characteristics that significantly improve predictive accuracy.

The results indicated that using only spectral and statistical features was insufficient across all earthquake scenarios. Instead, better anomaly detection was achieved when these features were vectorized in fixed intervals and their directional relationships were evaluated. This vector-based approach enhanced the performance of the LSTM deep learning model.

In scenarios involving near-focus sinusoidal movements caused by turbines, the vibrations were observed to excite specific frequencies in the bedrock, causing resonance. The identified frequency band persisted briefly after the turbine stopped abruptly, suggesting a resonance effect independent of the source. Remarkably, the same frequency range was also observed during earthquakes recorded in noise-free conditions, supporting the hypothesis that these frequencies are inherent to the bedrock's natural characteristics.

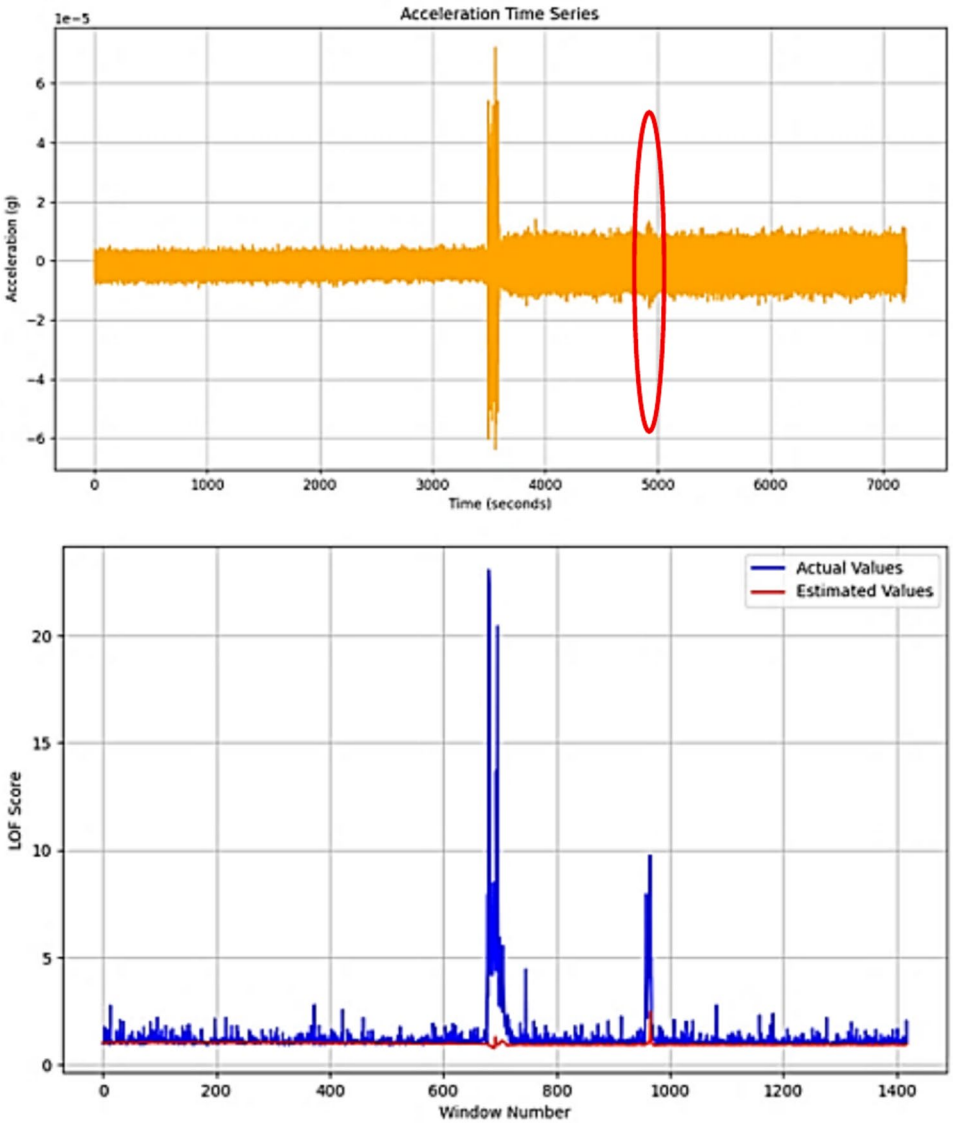


Fig. 27 Balıkesir earthquake record (21.03.2024): prediction of anomaly

The findings suggest that combinations of spectral and statistical features have significant potential for predicting seismic irregularities before their occurrence. These results can inform the design of advanced artificial intelligence models by providing a foundation for labeling earthquake-related anomalies. Additionally, they support the integration of attention mechanisms, offering valuable guidance for future academic research.

Building on these findings, the study introduces a novel framework that extends beyond traditional approaches in earthquake prediction. While traditional models often rely on simple parameters such as amplitude thresholds or sudden peaks in raw acceleration data, the proposed approach incorporates more detailed temporal and spectral information to enhance predictive capability.

The model employed 5-s sliding windows with 50% overlap to predict anomaly levels up to 50 s before an earthquake. Its effectiveness was evaluated using several performance metrics. The TPS was 64.4% to quantify the model's effectiveness, indicating its ability to detect actual seismic peaks correctly. The FPS was 17.5%, representing instances where non-seismic peaks were misclassified as seismic. The SSDS, which measures temporal accuracy, averaged 54.9%, showing moderate success in localizing actual seismic events in time. Additionally, the MAE in non-peak regions was 0.254. Given the normalized range of −1 to+1, this translates to a

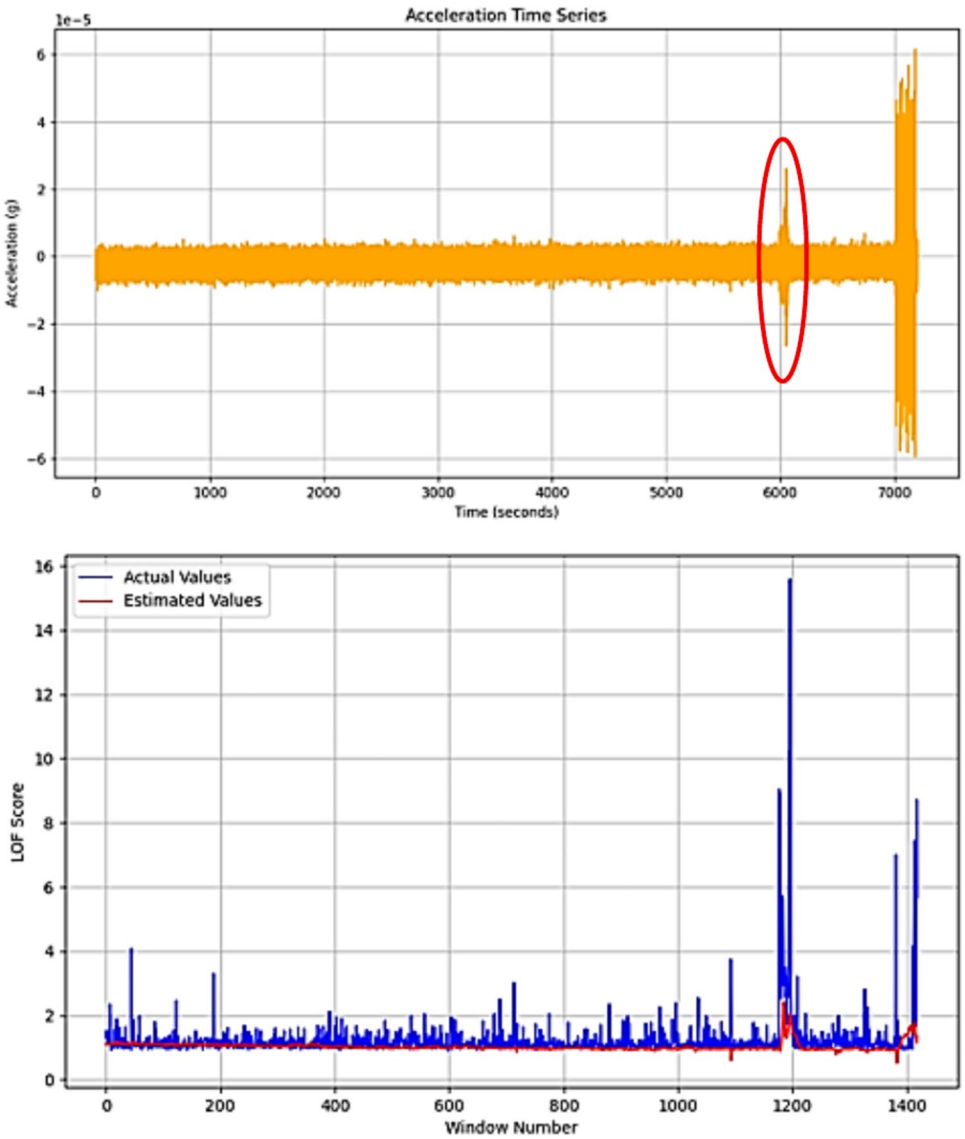


Fig. 28 Çanakkale earthquake record (04.03.2024): prediction of anomaly

25% average error. Although relatively high, this reflects the model's design to suppress background noise and prioritize meaningful signal peaks.

This study improves the model's learning capacity by incorporating a broad, multidisciplinary set of engineered features. Using LOF scores as regression targets allows the model to move beyond classical classification approaches. This enables it to represent pre-seismic anomalies as continuous and time-dependent patterns. The proposed framework contributes a novel approach to the literature, especially in identifying and tracking precursor seismic activity.

The proposed approach is not limited to issuing alerts at the onset of an earthquake; it also possesses the potential to anticipate precursor anomalies specific to the pre-seismic phase. In this regard, it provides a complementary analytical layer that enhances the responsiveness of existing early warning systems.

The model operates using only acceleration data, which enables the development of real-time, locally deployable systems at any sensor station. This offers a significant advantage for decentralized and distributed early warning architectures. Moreover, by employing LOF-based targeting and multidimensional feature combinations, the model has demonstrated stable performance even under noisy conditions. This is particularly advantageous for applications in industrial zones or dense urban sensor networks.

 https://doi.org/10.1007/s00521-025-11736-y

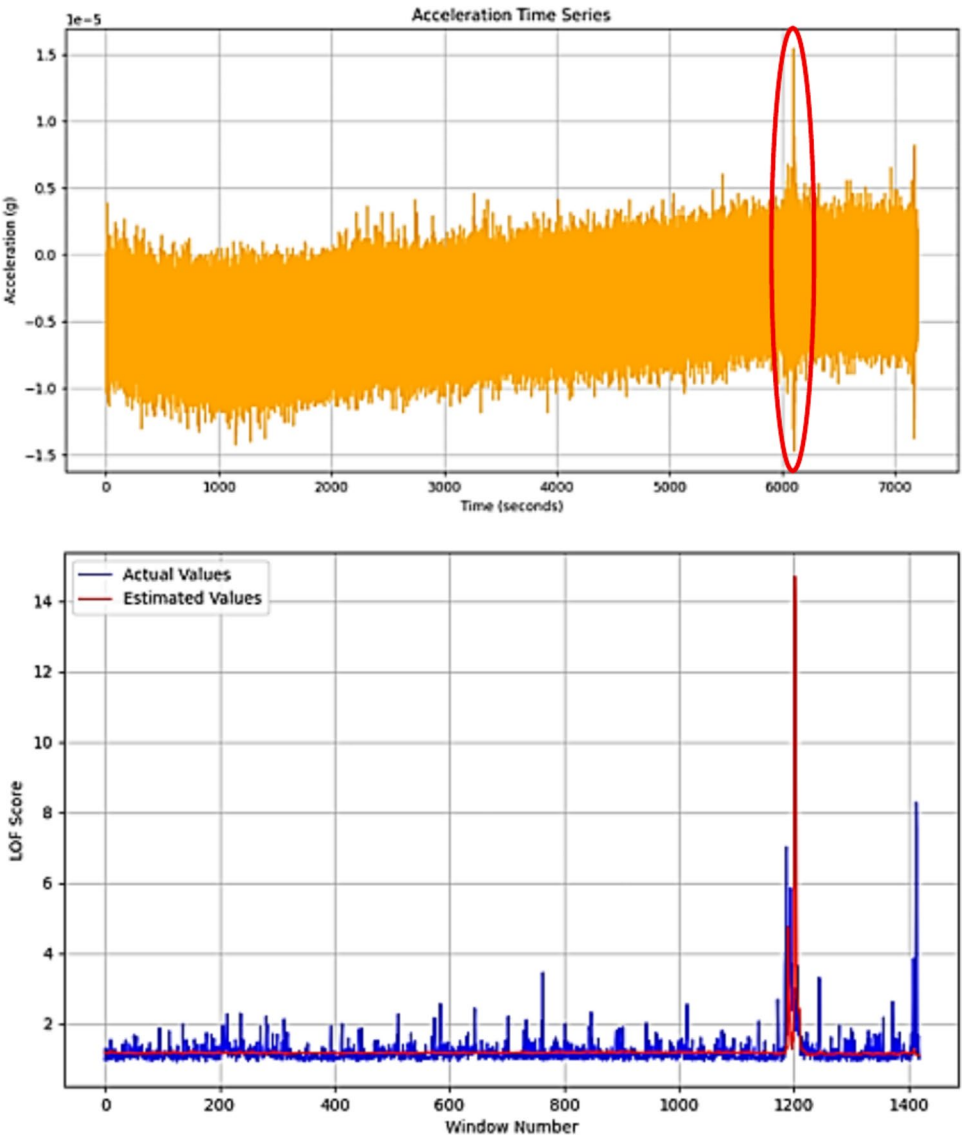


Fig. 29 Çanakkale earthquake record (22.07.2024): prediction of anomaly

In addition to early warning, the proposed method contributes to detecting and generalizing pre-seismic patterns. By learning temporal changes in features before earthquake peaks, the model captures event-specific behavioral signatures. This allows for the data-driven extraction of precursor patterns that are unique to particular regions or seismic events. Furthermore, its ability to identify similar patterns across different earthquake records highlights its capacity to learn generalizable seismic behaviors. Thus, the approach offers a robust framework for classifying precursor signals and comparing structural similarities among earthquakes across various regions.

Additionally, the model's sensitivity to pre-event patterns and its ability to evaluate complex feature combinations make it possible to distinguish non-seismic transient spikes—such as industrial explosions, impacts, or mechanical noise—from true seismic events. This capability reduces the likelihood of false alarms, enhancing the reliability and calibration of existing early warning systems.

In summary, the proposed method contributes to early warning systems in both preventative and corrective ways. It also deepens the scientific understanding of earthquake development processes and enables comparative analysis across multiple events, supporting broader generalization.

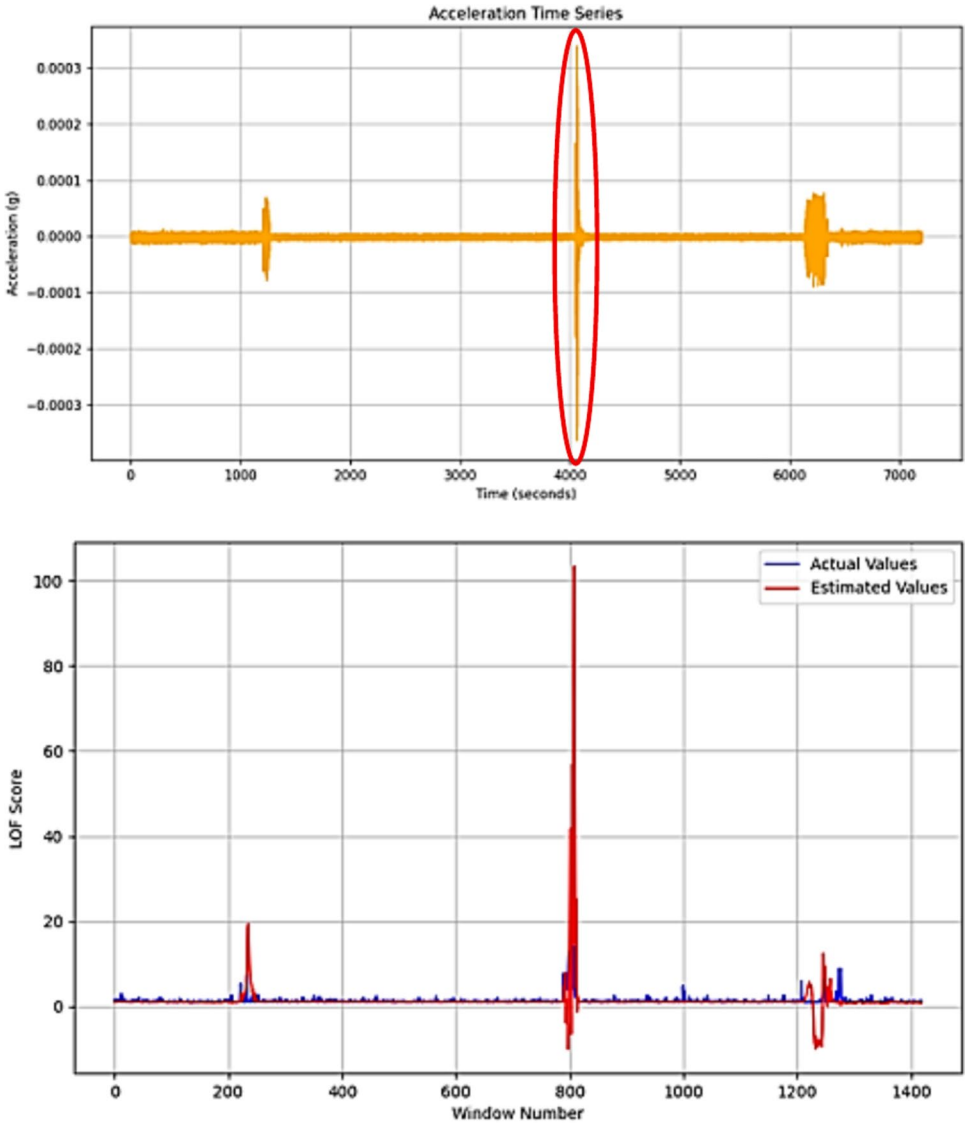


Fig. 30 Bolu earthquake record (14.10.2023): prediction of anomaly

5.1 Future work

In the current study, acceleration time-series data were reduced to representative features, and earthquake events were predicted based on these features. Future work will build on the findings of the feature engineering conducted in this study by incorporating additional features into the raw acceleration time-series data. This approach will enable earthquake prediction over longer-duration time-series data, enhancing the model's predictive capabilities.

Future research may involve comparing LSTM and other deep learning models to assess their performance and accuracy in these tasks, potentially incorporating approaches such as labeling earthquake moments or utilizing attention mechanisms.

In addition to the improvements made within the current acceleration-based framework, future studies aim to extend the model beyond its current structure by integrating GNSS and other geophysical data sources. With its capability to monitor crustal deformations at the millimeter scale, GNSS data enables the modeling of precursor processes such as slow slip events, surface stress accumulation, and displacement rate anomalies that occur prior to seismic activity. Simultaneous analysis of such deformation data alongside acceleration-based anomalies

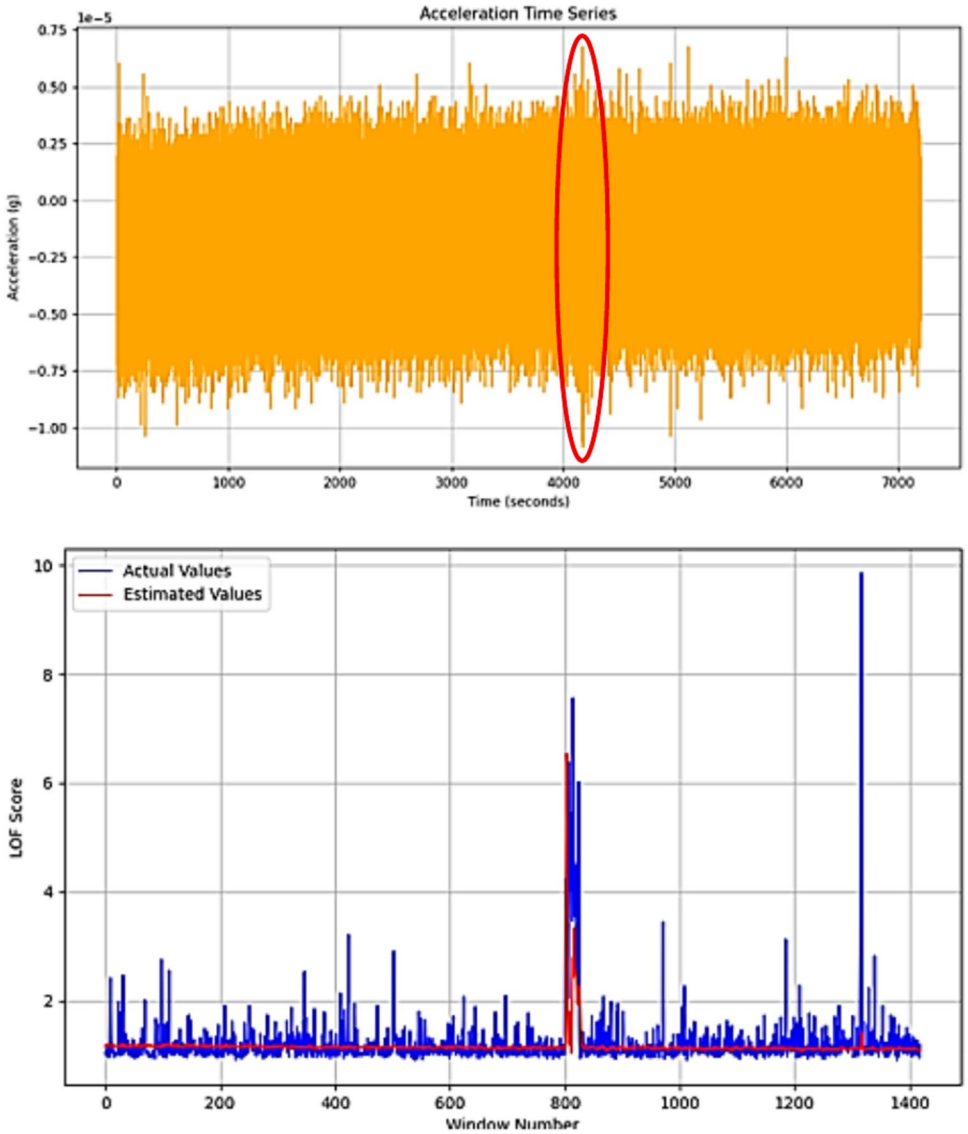


Fig. 31 Kozan earthquake record (27.10.2024): prediction of anomaly

would allow the model to be expanded to encompass the moment of the earthquake and the preceding processes leading up to it.

By jointly evaluating data from both acceleration and GNSS sources, a more comprehensive understanding can be achieved regarding the influence of bedrock motion on earthquake-generating mechanisms, the dynamics of earthquake propagation, and the complex causal relationships among triggered seismic features. This integrated approach would make it possible, through deep learning models, to infer temporally dependent multi-layered relationships between surface-level acceleration patterns and subsurface processes such as stress accumulation, slip rates, and deformation.

As a result, the predictive power of the model will improve, and the physical interpretation of earthquake generation processes will be significantly enhanced. In the future, deep learning models such as LSTM, or alternative architectures, can be retrained using multi-input channels (e.g., acceleration+GNSS), paving the way for interdisciplinary, data-driven integrated seismic monitoring systems.

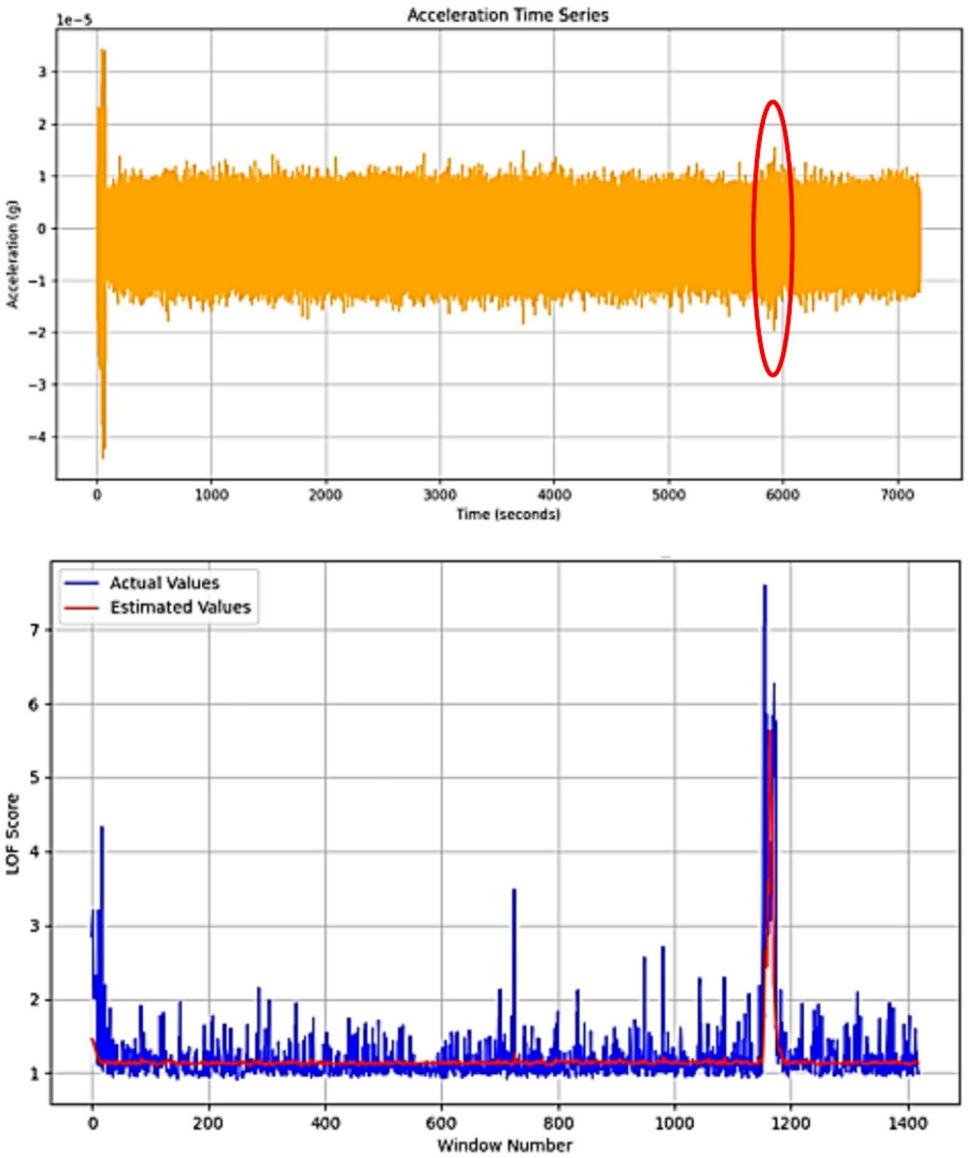


Fig. 32 Manisa earthquake record (24.06.2024): prediction of anomaly

 https://doi.org/10.1007/s00521-025-11736-y

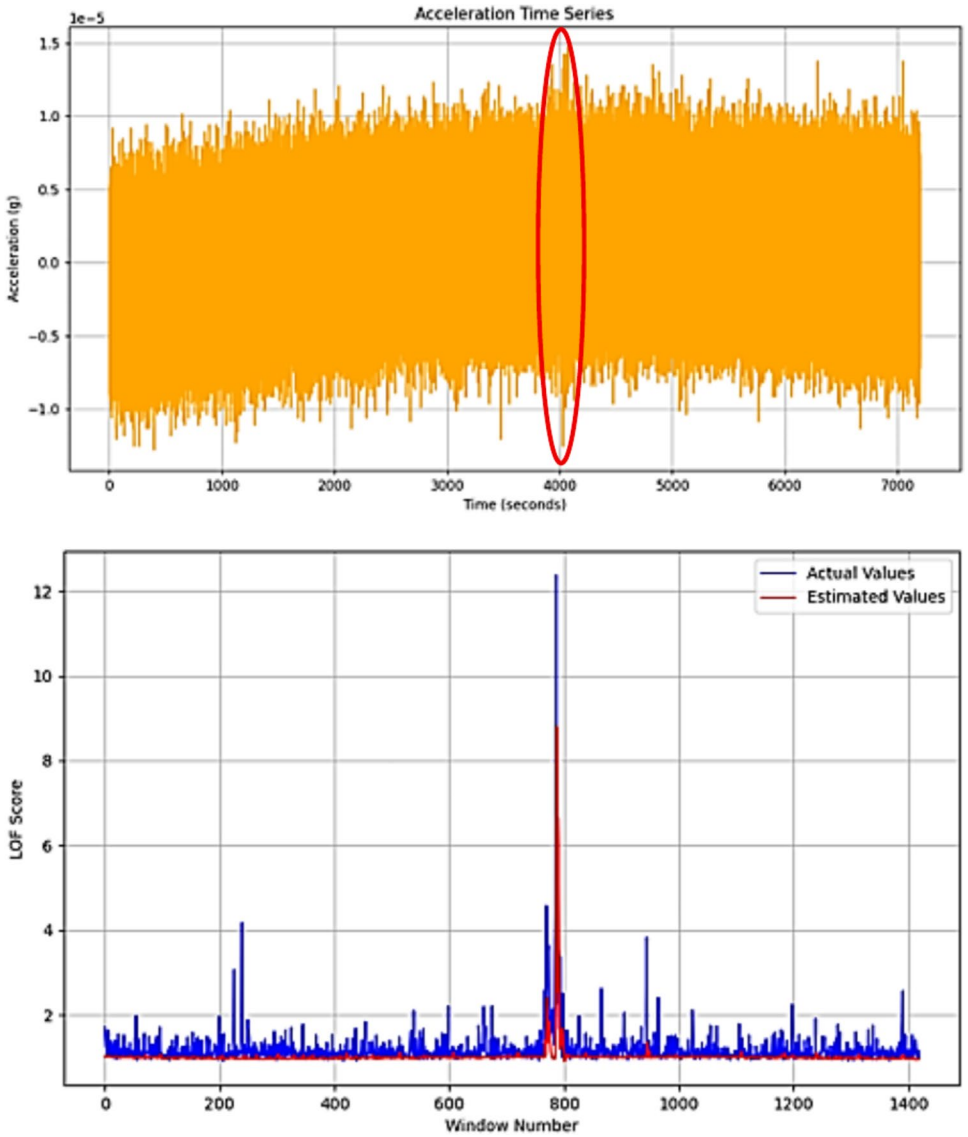


Fig. 33 Malatya earthquake record (25.01.2024): prediction of anomaly

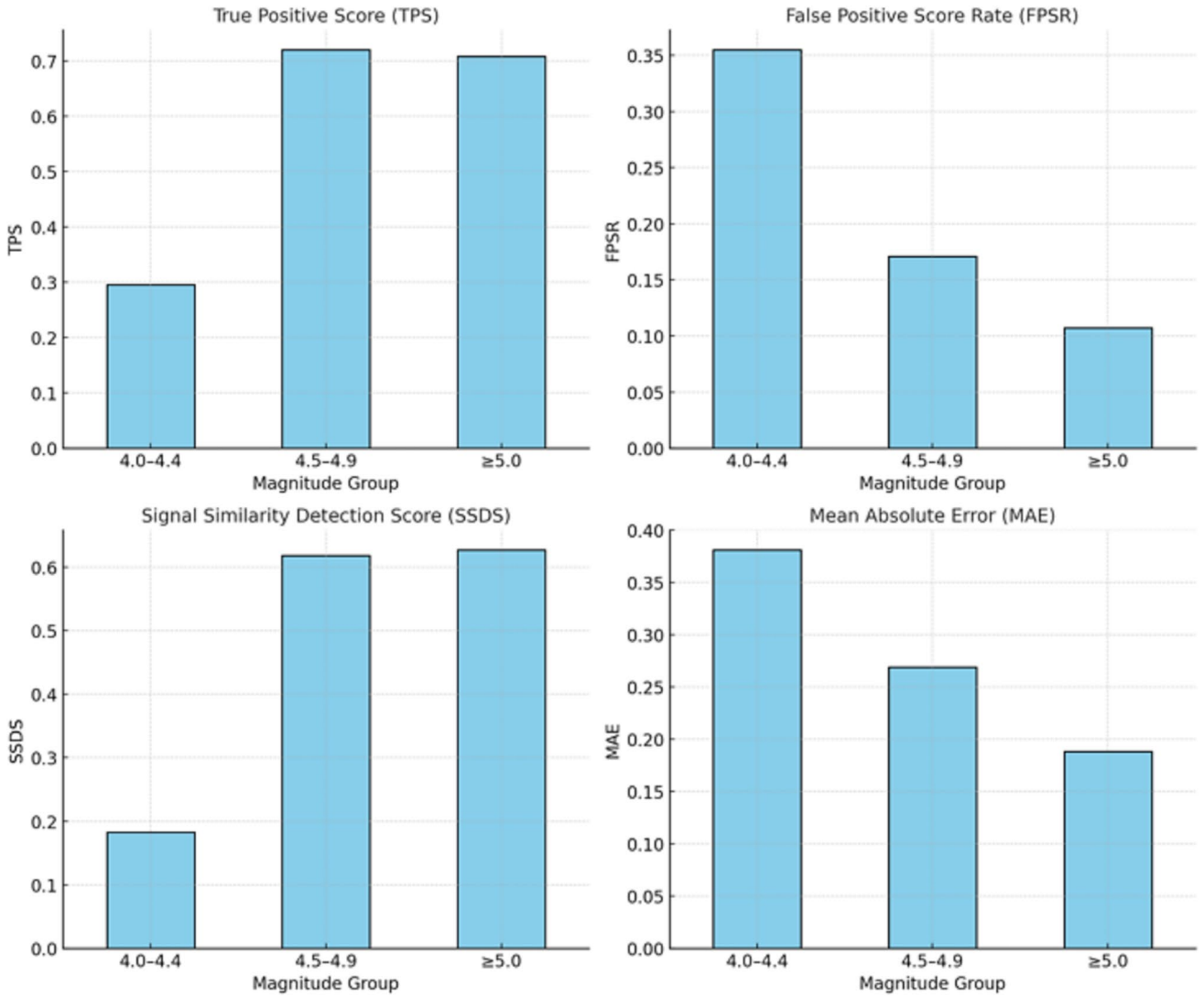


Fig. 34 Comparison of model performance metrics across earthquake magnitude groups

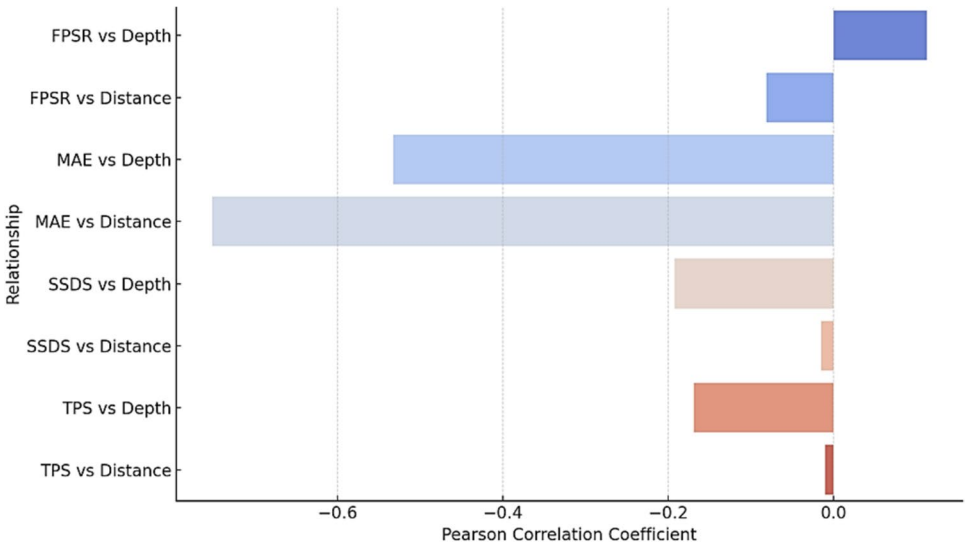


Fig. 35 Correlation between model metrics and earthquake depth/ distance

Acknowledgements This work is produced within the scope of the thesis study titled 'Bir Hidroelektrik Santrali Baraj Gövde Yapısının Operasyonel Modal Analizi (In Turkish)' (Operational Modal Analysis of a Hydroelectric Power Plant Dam Body Structure).

Funding Open access funding provided by the Scientific and Technological Research Council of Türkiye (TÜBİTAK). This work was supported by the PhD Project (FDK-2022–7891) funded by the Scientific Research Projects Coordination Unit (BAP), Gazi University.

Data availability The earthquake data used in this study are specific to certain site conditions and sensor locations, and are subject to commercial and operational sensitivities. Therefore, they are not publicly accessible. However, data requests made for academic research purposes will be considered, provided that a Non-Disclosure Agreement (NDA) is signed between the parties. Upon agreement, the data can be shared in.csv format. The source code used in this study is available at the following GitHub repository: https://github.com/grhntkgz/LSTM_Earthquake_Anomaly

Declarations

Competing interests The authors have no relevant financial or non-financial interests to disclose.

Open Access This article is licensed under a Creative Commons Attribution 4.0 International License, which permits use, sharing, adaptation, distribution and reproduction in any medium or format, as long as you give appropriate credit to the original author(s) and the source, provide a link to the Creative Commons licence, and indicate if changes were made. The images or other third party material in this article are included in the article's Creative Commons licence, unless indicated otherwise in a credit line to the material. If material is not included in the article's Creative Commons licence and your intended use is not permitted by statutory regulation or exceeds the permitted use, you will need to obtain permission directly from the copyright holder. To view a copy of this licence, visit http://creativecommons.org/licenses/by/4.0/.

References

1. AFAD (2023) 6 Şubat 2023 Pazarcık-Elbistan (Kahramanmaraş) Depremleri Raporu. Afet ve Acil Durum Yönetimi Başkanlığı. https://www.afad.gov.tr/6-subat-depremleri-bilgilendirme
2. Allen CR (1976) Seismological and geological factors in earthquake prediction. Proc Natl Acad Sci U S A 73(6):1709–1712
3. Mogi K (1968) Earthquake prediction and seismic gaps. Tectonophysics 5(1):35–42
4. Utsu T (1961) A statistical study on the occurrence of aftershocks. Geophys Mag 30:521–605
5. Abebe E, Kebede H, Kevin M, Demissie Z (2023) Earthquakes magnitude prediction using deep learning for the Horn of Africa. Soil Dyn Earthq Eng. https://doi.org/10.1016/j.soildyn.2023.107913
6. Shao Z, Wu Y, Ji L, Diao F, Shi F, Li Y, Long F, Zhang H, Wang W, Wei W, Wang P, Liu X, Liu Q, Pan Z, Yin X, Liu Y, Feng W, Zou Z, Cheng J, Lu R, Xu Y, Li X (2023) Assessment of strong earthquake risk in the Chinese mainland from 2021 to 2030. Earthq Res Adv. https://doi.org/10.1016/j.eqrea.2022.100177
7. Koehler J, Li W., Faber J, Rümpker G, Srivastava N (2024). Testing the potential of deep learning in earthquake forecasting. arXiv:2307.01812v1
8. Nicolis O, Plaza F, Salas R (2020) Prediction of intensity and location of seismic events using deep learning. Spat Stat. https://doi.org/10.1016/j.spasta.2020.100442
9. Jena R, Pradhan B, Naik SP, Alamri AM (2021) Earthquake risk assessment in NE India using deep learning and geospatial analysis. Geosci Front. https://doi.org/10.1016/j.gsf.2020.11.007
10. Mousavi SM, Beroza GC (2020) Bayesian-deep-learning estimation of earthquake location from single-station observations. IEEE Trans Geosci Remote Sens. https://doi.org/10.1109/TGRS.2020.2988770
11. Berhich A, Belouadha F-Z, Kabbaj MI (2023) An attention-based LSTM network for large earthquake prediction. Soil Dyn Earthq Eng. https://doi.org/10.1016/j.soildyn.2022.107663
12. Bhandarkar T, Vardaan K, Nikhil Satish S, Sridhar RS, Ghosh S (2019) Earthquake trend prediction using long short-term memory RNN. Int J Electr Comput Eng(IJECE). https://doi.org/10.11591/ijece.v9i2.pp1304-1312
13. Su Z, Zhang Q (2020) Earthquake prediction based on Bi-LSTM+CRF model and spatio-temporal data. In: 2020 IEEE 9th Jt Int Inform Technol Artif Intell Conf (ITAIC) 615(1):012008. 1109/ITAIC49862.2020.9339192
14. Wang C, Li C, Yong S, Wang X, Yang C (2022) Time series and non-time series models of earthquake prediction based on AETA data: 16-week real case study. Appl Sci. https://doi.org/10.3390/app12178536

15. Henríquez AC, Marin M, Pino OV et al (2022) End-to-end LSTM-based earthquake magnitude estimation with a single station. IEEE Trans Geosci Remote Sens. https://doi.org/10.1109/LGRS.2022.3175108
16. Abdalzaher MS, Soliman MS, Fouda MM (2024) Using deep learning for rapid earthquake parameter estimation in single-station single-component earthquake early warning system. IEEE Trans Geosci Remote Sens. https://doi.org/10.1109/TGRS.2024.3492023
17. Rusho MA, Azizova R et al (2024) Advanced earthquake prediction: unifying networks, algorithms, and attention-driven LSTM modelling. Geomate J 53(4):789–805
18. Wang Ao, Li S, Jianqi Lu, Zhang H, Wang B, Xie Z (2023) Prediction of PGA in earthquake early warning using a long short-term memory neural network. Geophys J Int. https://doi.org/10.1093/gji/ggad067
19. Wang C-Y, Huang T-C, Yih-Min Wu (2022) Using LSTM neural networks for onsite earthquake early warning. Seismol Res Lett. https://doi.org/10.1785/0220210197
20. Jia J, Ye W (2023) Deep learning for earthquake disaster assessment: objects, data, models, stages, challenges, and opportunities. Remote Sens. https://doi.org/10.3390/rs15164098
21. Chandrakumar C, Prasanna R, Stephens M, Tan ML (2022) Earthquake early warning systems based on low-cost ground motion sensors: a systematic literature review. Front Sens. https://doi.org/10.3389/fsens.2022.1020202
22. Rubidha DD, Govindarajan P, Venkatanathan N (2024) Towards real-time earthquake forecasting in Chile: integrating intelligent technologies and machine learning. Comput Electr Eng. https://doi.org/10.1016/j.compeleceng.2024.10928
23. Sapkota S (2023). Geological factors in dam site selection: importance of foundation rock, structures, and overburden. https://doi.org/10.13140/RG.2.2.10250.54720
24. Kramer SL (1996) Geotechnical earthquake engineering. Prentice Hall, Hoboken
25. Durante MG (2015) Experimental and numerical assessment of dynamic soil-pile-structure interaction. PhD Thesis. University of Naples Federico II.
26. Bernard M, Grant P, Thompson J (2002) Digital signal processing: concepts and applications. Palgrave Macmillan, New York
27. Aggarwal K, Mukhopadhyay S, Tangirala AK (2020) Statistical characterization and time-series modeling of seismic noise. arXiv. Published September 3.
28. Zhu W, Mousavi SM, Beroza GC (2018) Seismic signal denoising and decomposition using deep neural networks. arXiv. 2018. Published November 6.
29. Qasim M, Khan M, Mehmood W, Sobieczky F, Pichler M, Moser B (2022) A comparative analysis of anomaly detection methods for predictive maintenance in SME. In: Kotsis G et al (eds) Database and expert systems applications—DEXA 2022 workshops. DEXA 2022. Communications in computer and information science, vol 1633. Springer, Cham, pp 22–31. https://doi.org/10.1007/978-3-031-14343-4_3
30. Liu FT, Ting KM, Zhou ZH (2008) Isolation Forest. In: 2008 Eighth IEEE Int Conf Data Min. Pisa, Italy, pp 413–422. https://doi.org/10.1109/ICDM.2008.17.
31. Schölkopf B, Platt JC, Shawe-Taylor J, Smola AJ, Williamson RC (2001) Estimating the support of a high-dimensional distribution. Neural Comput 13(7):1443–1471. https://doi.org/10.1162/089976601750264965

Publisher's Note Springer Nature remains neutral with regard to jurisdictional claims in published maps and institutional affiliations.

Authors and Affiliations

Gürhan Tokgöz[1] · Eda Avanoğlu Sıcacık[2]

✉ Eda Avanoğlu Sıcacık
eavanoglu@gazi.edu.tr

Gürhan Tokgöz
grhntkgz@gmail.com

[1] Department of Civil Engineering, Graduate School of Natural and Applied Sciences, Gazi University, 06570 Ankara, Turkey

[2] Department of Civil Engineering, Faculty of Technology, Gazi University, 06570 Ankara, Turkey